

**Device modelling and optimization of lead-Free
(NH₄)₃Sb₂I₉ perovskite solar cells by using
SCAPS-1D**

A DISSERTATION

**SUBMITTED IN PARTIAL FULFILMENT OF THE REQUIREMENTS
FOR THE AWARD OF THE DEGREE
OF**

**MASTER OF SCIENCE
in
Physics**

**by
SUMIT SINGH
(23/MSCPHY/47)**

**Under the Supervision of
Dr. SARITA BAGHEL
Assistant Professor**



**Department of Applied Physics
DELHI TECHNOLOGICAL UNIVERSITY
(Formerly Delhi College of Engineering)
Shahbad Daulatpur, Main Bawana Road, Delhi- 110042
June 2025**

DECLARATION

I, **Sumit Singh (23/MSCPHY/47)** hereby certify that the work which is presented in Dissertation-II entitled “Device modelling and optimization of lead-free $(\text{NH}_4)_3\text{Sb}_2\text{I}_9$ perovskite solar cells by using SCAPS-1D” in fulfilment of the requirement for the award of the Master in Science in Physics and submitted to the Department of Applied Physics, Delhi Technological University, Delhi is an authentic record of my own, carried out during a period from August 2024 to May 2025 under the supervision of **Dr. Sarita Baghel**.

The matter presented in this report/thesis has not been submitted by me for the award of any other degree of this or any other Institute/University. The work has been accepted in SCIE indexed Journal with the following details:

Title of paper: “Device modelling and optimization of lead-free $(\text{NH}_4)_3\text{Sb}_2\text{I}_9$ perovskite solar cells by using SCAPS-1D”.

Author names (in sequence as per research paper): Sumit Singh, Rahul Kundara, Sarita Baghel.

Name of the Journal: Physica Scripta, IOP Science

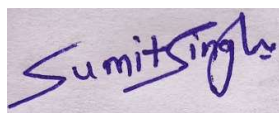
Status of paper (Accepted/Published): Accepted

Date of paper communication: March 15, 2025

Date of paper acceptance: June 2, 2025

Date of paper publication:

Sumit Singh (23/MSCPHY/47)



SUPERVISOR CERTIFICATE

To the best of my knowledge, this work has not been submitted in part or full for any Degree or Diploma to this University or elsewhere. I further certify that the publication and indexing information given by the student is correct.



Place: Delhi

Date: June 8, 2025

Dr. Sarita Baghel

SUPERVISOR

Assistant Professor

Department of Applied Physics

ABSTRACT

As commercialization and industrial growth continue to accelerate, the demand for power and energy is rising steadily. Growing energy needs can be responsibly met while protecting the environment for coming generations by using renewable energy. With proper harvesting, solar power becomes not just viable—but one of the most effective renewable energy options. This makes it crucial to enhance solar technologies that are both high-performing and safe for the environment. Advancing lead-free perovskite solar cells (PSCs) is essential for developing sustainable and eco-friendly solar technologies. These alternatives to lead-based PSCs offer notable benefits, including low cost, excellent stability and promising efficiency positioning them as attractive candidates for next-generation photovoltaic applications. Among the emerging materials, $(\text{NH}_4)_3\text{Sb}_2\text{I}_9$ stands out due to its favourable optoelectronic properties and environmental safety. This study investigates the impact of different HTLs and ETLs on the performance of a $(\text{NH}_4)_3\text{Sb}_2\text{I}_9$ -based device using SCAPS-1D software. Several parameters influencing device efficiency were optimised, including thickness of absorber layer, operating temperature, work function of back contact, donor density, defect density (N_t), series and shunt resistance. The optimized device structure $\text{FTO}/\text{WS}_2/(\text{NH}_4)_3\text{Sb}_2\text{I}_9/\text{MASnBr}_3/\text{Au}$ achieved a PCE of 20.08 % (with a V_{OC} of 1.65 V, JSC of 13.83 mA/cm^2 and FF of 87.93 %) at 300 K and N_t of 10^{13} cm^{-3} . These results demonstrate the strong potential of antimony-based perovskites in the development of high-performance, lead-free solar cells.

ACKNOWLEDGEMENTS

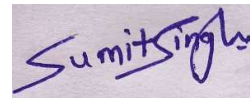
I sincerely thank **Dr. Sarita Baghel** Ma'am for her unwavering support, insightful guidance, and constant encouragement during my M.Sc. Dissertation II. Her profound knowledge and thoughtful suggestions have significantly contributed to the depth and quality of my research. I remain truly inspired by her commitment to nurturing academic excellence in her students.

I am also thankful to **Mr. Rahul Kundara**, Ph.D. scholar, for his continuous guidance and mentorship throughout the semester. From helping me understand how to conduct a thorough literature review to guiding me through the process of writing a research paper and responding to reviewer comments during revisions, his support has been indispensable. I have learned a great deal under his mentorship, and his patience and dedication have significantly contributed to the successful completion of my dissertation.

I am also deeply thankful to the **Department of Applied Physics at Delhi Technological University** for offering vital resources and a nurturing environment that greatly supported my research work. I truly appreciate the faculty and staff for their valuable assistance and knowledge, which significantly enhanced my academic journey.

I am equally grateful to my classmates and colleagues for their collaboration and support; our engaging discussions played a key role in shaping my ideas and expanding my outlook. I also acknowledge the use of SCAPS-1D software, developed by the University of Gent, Belgium, which was crucial to the simulation aspect of my research.

In conclusion, I thank Dr. Sarita Baghel, Mr. Rahul Kundara, the Department of Applied Physics, and all those who contributed to the success of our dissertation and academic journey.



SUMIT SINGH
(23/MSCPHY/47)

CONTENTS

Title	Page No.
Declaration and Supervisor's Certificate	ii
Abstract	iii
Acknowledgments	iv
Table of Contents	v-vi
List of Tables	vii
List of Figures	viii
List of Symbols and Abbreviations	ix
 CHAPTER 1 - INTRODUCTION	 1-6
1.1 Overview	01
1.2 Global Trend of Renewable Energy	02
1.3 Why Solar Energy	03
1.4 Photovoltaic Cell and its Types	03
1.5 Objective and Scope	06
 CHAPTER 2 - LITERATURE REVIEW	 7-11
2.1 Overview: Perovskite Solar Cell	07
2.2 Problem with lead-based PSCs	08
2.3 Antimony-based PSC	09
2.4 Why we choose $(\text{NH}_4)_3\text{Sb}_2\text{I}_9$ as absorber material	09
2.5 About SCPAS-1D Software	10
 CHAPTER 3 - METHODOLOGY	 12-19
3.1 Overview: Procedure	12
3.2 Device Structure and Simulation	17

CHAPTER 4 -	RESULTS AND DISCUSSION	20-33
4.1 Optimization of Appropriate ETL and HTL.....	20	
4.2 Impact of defect density.....	23	
4.3 Impact of thickness	25	
4.4 Impact of operating temperature on device performance	26	
4.5 Impact of Doner Density	27	
4.6 Impact of Series and Shunt Resistance	27	
4.7 Impact of back contact on PSC.....	28	
4.8 Comparison with Previous Reported Results	30	
4.9 Feasibility of fabricating the proposed structure and strategies to improve PSCs	33	
CHAPTER 5-	LEARNING THROUGH THE PROCESS OF RESEARCH PAPER WRITING	34-35
CHAPTER 6 -	CONCLUSION	36
REFERENCE		37-40
APPENDICES		41-45
A.1 Proof of Submission and Status of Paper.....	41	
A.2 Proof of SCI/SCIE/SCOPUS indexing	43	
A.3 Plagiarism Report.....	44	

LIST OF TABLES

CHAPTER 3

Table 3.1 Initial input parameter of PSCs

Table 3.2 Parameters for simulation of different

Table 3.3 Parameters for simulation of different ETLs.

Table 3.4 Various Device Structures and their simulation results.

CHAPTER 4

Table 4.1 Work Function of different electrodes.

Table 4.2 Comparison of Initial and Optimized Device Structure.

Table 4.3 Comparison with the previously reported work.

LIST OF FIGURES

CHAPTER 1

Figure 1.1 Pictorial view of (a) renewable and (b) non-renewable energy sources.

Figure 1.2 Share of renewable electricity generation by technology, 2000-2030 (IAE)

Figure 1.3 Photovoltaic Cell

Figure 1.4 Types of Photovoltaic solar cells

Figure 1.5 Overview of the highest recorded efficiencies for different photovoltaics technologies

CHAPTER 2

Figure 2.1 Cristal Structure of cubic PSC.

Figure 2.2 Device Structure of PSC.

CHAPTER 3

Figure 3.1 Simulation Procedure.

Figure 3.2 Device Structure and energy band diagram for $(\text{NH}_4)_3\text{Sb}_2\text{I}_9$ -based PSC.

CHAPTER 4

Figure 4.1 Energy band diagram of absorber layer with different (a) HTLs and (b) ETLs.

Figure 4.2 J-V and QE characteristics of distinct HTLs with WS_2 as ETL.

Figure 4.3 J-V and QE characteristics of distinct HTLs with TiO_2 as ETL.

Figure 4.4 J-V and QE characteristics of distinct HTLs with PCBM as ETL.

Figure 4.5 J-V and QE characteristics of distinct HTLs with IGZO as ETL.

Figure 4.6 The impact of defect density on performance parameters of PSC.

Figure 4.7 Impact of thickness of Absorber layer on performance parameters.

Figure 4.8 Impact of Temperature on $(\text{NH}_4)_3\text{Sb}_2\text{I}_9$ -based PSC.

Figure 4.9 Impact of acceptor density on $(\text{NH}_4)_3\text{Sb}_2\text{I}_9$ -based PSC

Figure 4.10 Impact of (a) R_s at $R_{sh} = 10^5 \text{ } (\Omega\text{-cm}^2)$ and (b) R_{sh} at $R_s = 0.5 \text{ } (\Omega\text{-cm}^2)$ on performance parameter of PSC

Figure 4.11 Band gap energy of PSC vs distinct back contact. (a) C, Au, Ni (b) Pt.

Figure 4.12 (a) J-V of the device for distinct back contact. (b) PCE and FF for distinct back contact.

Figure 4.13 J-V and QE curve for initial and optimized PSC

Figure 4.14 Band offsets (Spike, Cliff) diagram of optimised device.

Figure 4.15 Absorption coefficient plot of WS_2 , PCBM, MASnBr_3 , and $(\text{NH}_4)_3\text{Sb}_2\text{I}_9$ layers.

LIST OF SYMBOLS

<u>Symbol</u>	<u>Description</u>
J_{sc}	Short Circuit Current
V_{oc}	Open Circuit Voltage
E_g	Bandgap
χ	Electron Affinity
N_c	Effective density of states in the conduction band
N_v	Effective density of states in the valence band
N_D	Concentration of donor impurities
N_A	Concentration of acceptor impurities
N_t	Defect density

LIST OF ABBREVIATIONS

<u>Abbreviations</u>	<u>Description</u>
PSC	Perovskite Solar Cell
FF	Fill Factor
PCE	Power Conversion Efficiency
HTL	Hole Transport Layer
ETL	Electron Transport Layer
SCAPS-1D	Solar Cell Capacitance Simulator 1D
FTO	Fluorine-doped Tin Oxide

Chapter 1

Introduction

1.1 Overview

Human survival and progress have always depended on resources like water, minerals, and energy. Meeting energy demand with limited fossil fuels isn't sustainable. To ensure long-term growth and environmental protection, we must transition efficiently to renewable energy sources. This shift is crucial to reduce reliance on depleting reserves and support a more sustainable future.

Renewable and Non-renewable sources both are used in energy generation but the things that differentiate them is the regeneration within the time scale. Non-renewable energy cannot be replaced within a human time scale once used that means they are in limited quantities and take millions of years in formation. They also cause pollution and other environmental effects. On the other hand, renewable energy comes from natural sources that do not run over time. They are sustainable and environment-friendly. They are listed in fig. (1.1).

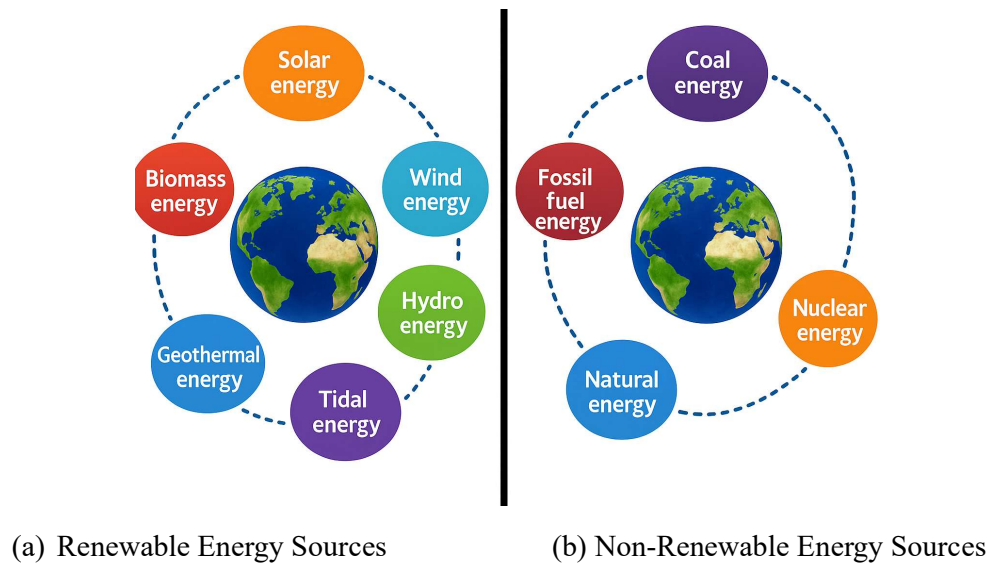


Fig.1.1 Pictorial view of (a) renewable and (b) non-renewable energy sources.

As commercialization and industrial growth continue to accelerate, the demand for power and energy is rising steadily. Using conventional fuels like natural gas, oil, and fossil fuels depletes our finite resources and harms the environment. This emphasizes the importance

of seeking and adopting renewable energy alternatives. Growing energy needs can be responsibly met while protecting the environment for coming generations by using renewable energy.

1.2 Global Trend of Renewable Energy

The global energy landscape has changed significantly between 2008 and 2025, with renewable sources gaining a much larger share of the total energy mix as shown in fig. (1.2). In 2008, renewables accounted for 18.6%, which grew to 34.5% by 2025. Although hydropower remained a key contributor, its share dropped slightly from 15.9% to 14.2%, suggesting a broader shift toward other renewable technologies.

The most striking development during this period was the rapid rise of variable renewables, particularly solar photovoltaic (PV) and wind energy. From a combined share of just 1.2% in 2008, they expanded to 17.5% by 2025. Wind energy grew from 1.1% to 9.2%, and solar PV increased from a minimal 0.1% to 8.3%. This remarkable growth can be attributed to continuous technological improvements, supportive government policies, and a sharp decline in generation costs. Other renewable sources also saw moderate growth—from 1.5% to 2.8%—further contributing to the diversification of clean energy.

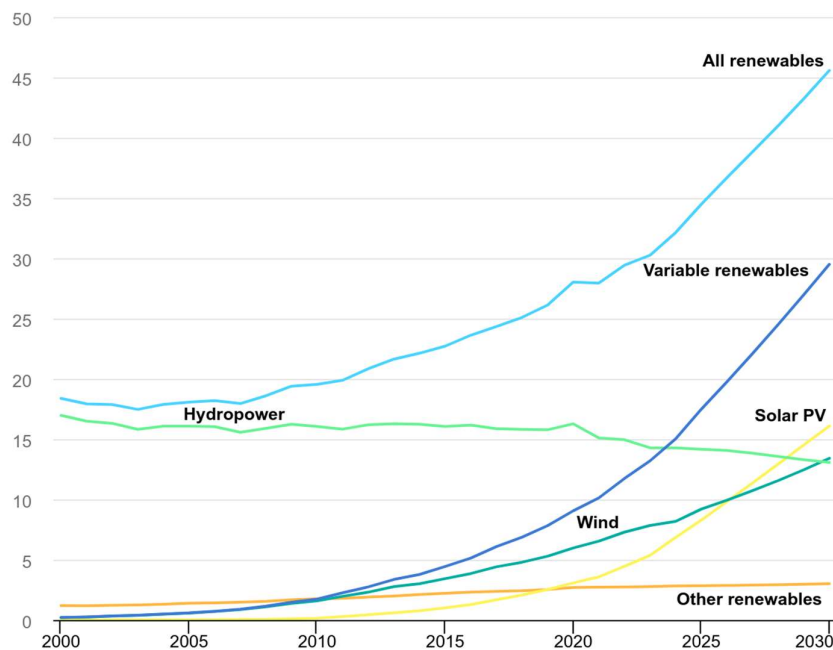


Fig. 1.2 Diversification of clean energy, 2000-2030 (IAE) ^[48]

Overall, the data reflects a global transition away from a hydro-dominated renewable mix toward one where solar plays a central role. This shows the increasing need for decentralized and sustainable energy solutions to tackle climate change and improve energy security.

Given this momentum, it becomes essential to understand the unique advantages of solar energy. Its rapid adoption across the globe highlights its potential to become a cornerstone of future energy systems. This leads to the next discussion—why solar energy is emerging as a key solution in the clean energy transition.

1.3 Why Solar Energy?

With proper harvesting, solar power becomes not just viable—but one of the most effective renewable energy options. As in just 1.5 days, the sun generates 1.7×10^{22} joules of energy, which is same as total energy stored in 3 trillion barrels of Earth's oil reserves [1]. This highlights that the sun alone can easily fulfil humanity's energy needs and makes solar energy as the top contender among renewable resource—clean, accessible, abundant, and environmentally friendly. Solar energy offers immense potential for practical use through technologies like thermoelectric, photocatalytic, photovoltaic (PV), and photoelectrochemical (PEC) systems. Among these, PV technology stands out as a key approach for directly converting sunlight into electricity, making it a vital tool in harnessing solar power for sustainable energy solutions.

1.4 Photovoltaic Cell and it's types

PV cell turns sunlight into electricity through layered semiconductor materials and electric field-driven charge separation. When sunlight hits the cell, photons knock electrons loose in the silicon. The built-in electric field at the p-n junction then pushes these electrons toward n-side (front contact) and holes toward p-side (back contact), enabling current flow. It is shown in below fig. (1.3).

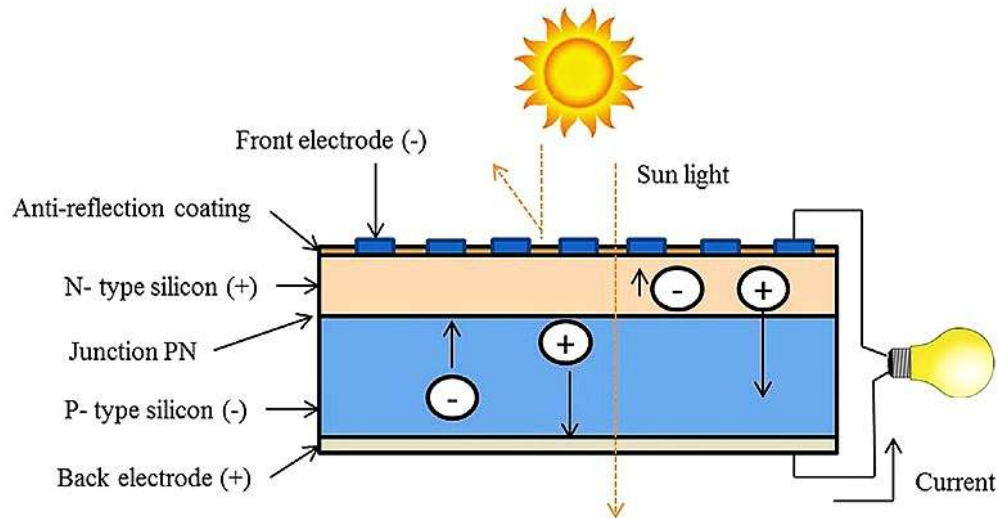


Fig. 1.3 Photovoltaic Cell^[49]

PV technologies are advancing rapidly in both research and commercial sectors. Solar cell technology has evolved through three major generations based on how the technology has evolved, the materials used, their efficiency, and overall cost. It is shown in fig (1.4).

The first one is first generation consists of SSCs, which have become the most established and widely used PV technology, currently holding over 90% of the global PV market. Crystalline silicon cells now achieve PCE exceeding 20%, with single-crystalline types reaching up to 26.6%.

The next one is Second-generation PV technologies that include thin-film solar cells like CIGS, CdTe, and GaAs. These have shown impressive PCEs of 28.8%, 22.1%, and 22.6%, respectively.

The third generation features emerging technologies such as DSSC, PSCs and quantum dot, which offer promising advantages like lower production costs. DSSCs have achieved up to 13% efficiency along with proven durability under accelerated aging tests.

Silicon solar cells have long dominated market, but they come with limitations like high production energy, efficiency limits, rigidity, and environmental concerns. On the other hand, perovskite and other next-gen solar technologies bring several advantages: higher efficiency potential, low-cost flexible fabrication, and better integration options. Their versatility, lightweight nature, and tunable properties make them essential for advancing solar technology beyond silicon's physical and economic limits.

The PSCs attract major attention due to their outstanding photovoltaic performance, flexible and adjustable band gap, and straightforward manufacturing process. The efficiency of PSCs has seen remarkable progress, rising from initially 3.8 % in 2009 to an impressive 27.0 % today as shown in fig. (1.5) [2].

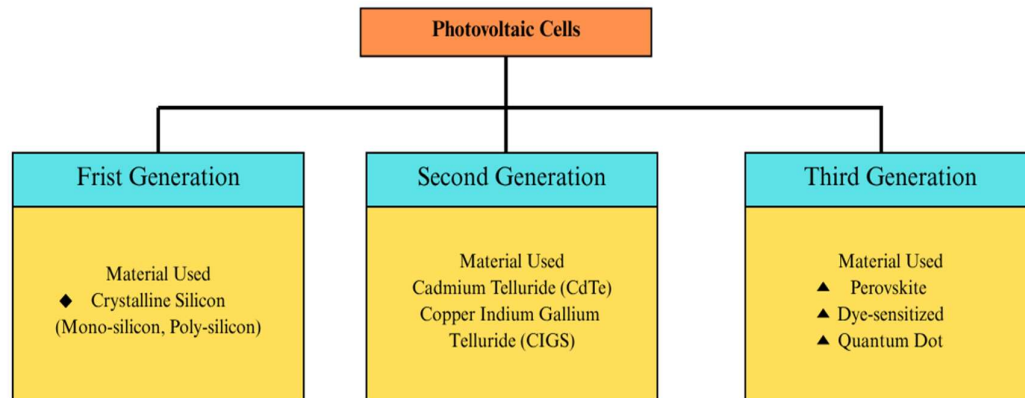


Fig. 1.4 Types of Photovoltaic solar cells

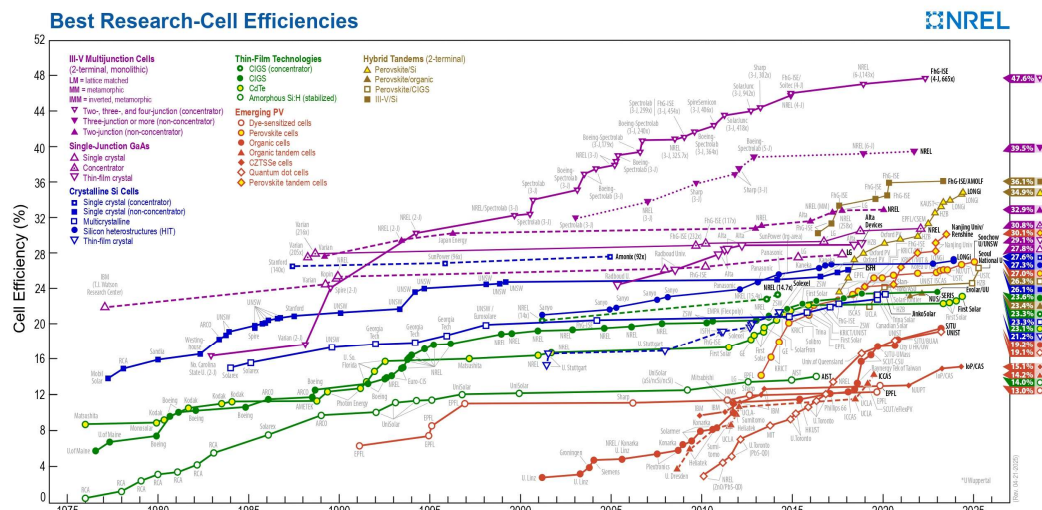


Fig. 1.5 Overview of the highest recorded efficiencies for different photovoltaic technologies^[2].

1.5 Objective and Scope

This thesis is about modelling and optimization of Sb-based, specifically using $(\text{NH}_4)_3\text{Sb}_2\text{I}_9$ as the absorber layer.

To achieve this objective, the project includes simulating and studying the factors that affect PSC devices. The scope of this thesis is divided as follows:

1 . Material Selection and Device Structure Design

- (a) Selection of $(\text{NH}_4)_3\text{Sb}_2\text{I}_9$ as a stable, environmentally friendly absorber material.
- (b) Exploration and justification of suitable ETLs and HTLs, with a focus on energy level alignment, mobility, and interface properties.

2. Numerical Simulation using SCAPS-1D

- a) Building device architecture using software.
- (b) Simulating the J-V characteristics, QE, and energy band.
- (c) Extracting key parameters: V_{OC} , J_{SC} , FF, and PCE.

3. Performance Comparison of Different HTLs/ETLs

- (a) Comparison between different device structure.
- (b) Selection of the most suitable combination for highest efficiency.

4. Optimization of Device Parameters

- (a) Systematic variation of layer thicknesses of absorber.
- (b) Analysis of defect density effects in each layer.
- (c) Investigating the effect of temperature.
- (d) Investigation the effect of back contact work function and series/shunt resistances.

Chapter 2

Literature Review

2.1 Overview: Perovskite Solar Cell

Perovskite materials are a group of compounds with the general formula ABX_3 . Here, 'A' is a positively charged ion like methylammonium, formamidinium, or cesium; 'B' is usually a metal ion with a +2 charge, often lead or tin; and 'X' is a halide ion such as chloride, bromide, or iodide. These materials are great for solar cells because they absorb light strongly, let electric charges move easily, and have long distances over which charges can travel without recombining. The term "perovskite" in this context refers to the structure rather than a specific chemical composition. Ideally, perovskites have a perfect cubic crystal shape as shown in fig. (2.1), but in real life, they often get a bit distorted or tilted because the sizes of the ions don't always fit perfectly. This distortion changes how the material behaves in terms of light absorption, electricity, magnetism, and other properties.

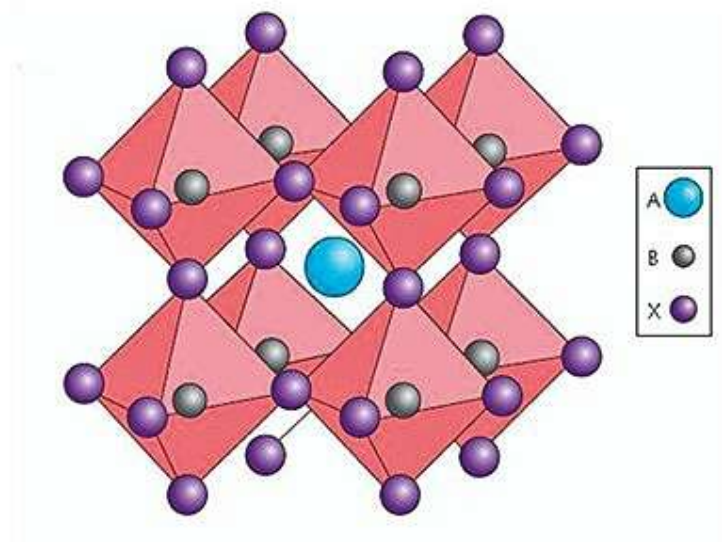


Fig. 2.1 Cristal Structure of cubic PSC^[5a]

Perovskite materials are just the absorbing material that helps in photoelectron generation. Along with the other layers like ETL, HTL, FTO and back contact, it forms a Perovskite solar cell. Each layer has its own function.

The working of PSCs relies on a series of charge-transfer processes. When exposed to light, the perovskite absorber generates electron-hole pairs through photoexcitation. Electrons are extracted by the ETL and flow toward FTO electrode, while holes are transferred to metal electrode via HTL. This separation of charges builds a potential difference between front and back contacts, allowing current to flow through an external circuit.

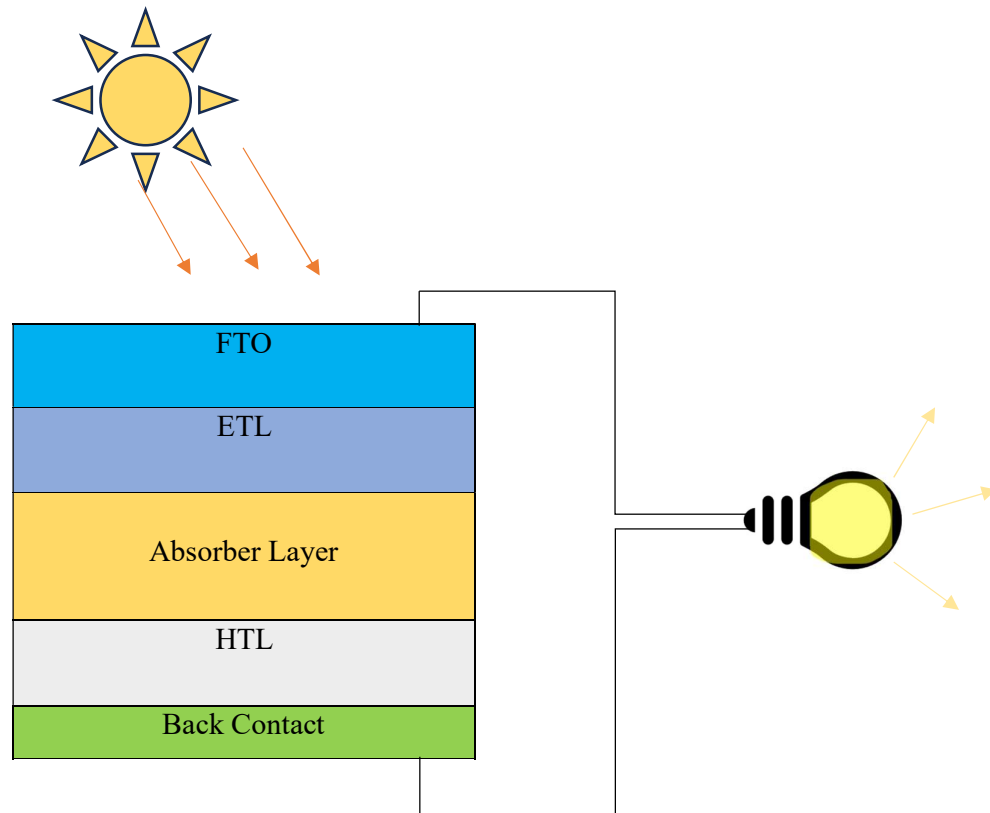


Fig. 2.2 Device Structure of PSC

2.2 Problem with lead-based PSCs and its alternative

As discussed above in the perovskite structure (ABX_3), 'B' is commonly Pb and they are known as Lead-based PSCs. Lead-based PSCs have sustainability problems because Pb is highly toxic and poses serious threats to both living organisms and the environment. Hence, it is crucial to explore more sustainable and efficient materials with lower toxicity to substitute lead (Pb) in PSCs. Recently, scientists have investigated eco-friendly metal elements that share characteristics with Pb, such as tin (Sn) [3], germanium (Ge) [4], and

antimony (Sb) [5], as potential substitutes in the absorber layer. Tin is naturally abundant and is safe for the environment and health, as it is not as harmful as Pb. Moreover, tin-based perovskites have a bandgap that aligns more closely with optimal range predicted by Shockley-Queisser limit theory offering an advantage over their lead-based counterparts [6]. However, tin faces a major challenge, as Sn^{2+} can easily oxidize to Sn^{4+} [7]. This limits the stability of Sn-based PSCs, hindering their long-term performance. Germanium, like lead, shares the same group in periodic table and has a smaller ion radius, which improves its ionic conductivity, but germanium-based perovskites are even more susceptible to oxidation than their tin-based counterparts due to the weaker inert pair effect [8], making their stability a critical drawback. Antimony, on the other hand, shares same ns^2 outer electronic configuration as lead and is considerably safer.

2.3 Antimony-Based PSC

Sb-based perovskite materials exhibit comparable optoelectronic properties to lead halide perovskites [9]. These qualities position antimony as a promising and viable substitute for lead in metal halide perovskites, offering a safer and more sustainable option for future advancements. My work is even on the Sb-based PSCs. The material that I have choosed for the research work is $(\text{NH}_4)_3\text{Sb}_2\text{I}_9$.

Here there could be the question that $(\text{NH}_4)_3\text{Sb}_2\text{I}_9$ does not resemble with ABX_3 structure then why it is PSC. The reason for this is although $(\text{NH}_4)_3\text{Sb}_2\text{I}_9$ does not adopt the typical 3D ABX_3 perovskite structure, it is considered a perovskite-like material due to its structural similarity at the octahedral level and its promising optoelectronic properties.

2.4 Why we choose $(\text{NH}_4)_3\text{Sb}_2\text{I}_9$ as absorber material

$(\text{NH}_4)_3\text{Sb}_2\text{I}_9$ perovskite layer has better conductivity and Sb-based materials often show lower defect formation energy and better tolerance to halide vacancies. Sb-based perovskite like $(\text{NH}_4)_3\text{Sb}_2\text{I}_9$ are more moisture-stable than lead-based ones because of strong chemical bond with halide ions than lead does. The NH_4^+ cations can form hydrogen bonds with water, potentially acting as a buffer and limiting moisture ingress into the perovskite lattice. In addition to this, there's a clear gap in current research very few simulation-based studies have been done on $(\text{NH}_4)_3\text{Sb}_2\text{I}_9$ for solar cell applications. This

work aims to address that gap and provide a theoretical understanding of its device-level performance through numerical simulation.

In 2021, P. Kumar et al. [10] prepared a thin film layer of $(\text{NH}_4)_3\text{Sb}_2\text{I}_9$ by two-step deposition method, which showed good stability. In 2023, Valli et al. [11] conducted structural and optoelectronic investigations on the $(\text{NH}_4)_3\text{Sb}_2\text{I}_9$ material in a low-temperature range and suggested its potential for photovoltaic applications. Fabricating the various layers of a PSC through experimental methods is both time-intensive and costly. As a result, computational modelling and simulation play a vital role in identifying optimal materials for each layer of PSCs. The absorber layer's efficiency can be improved by selecting appropriate electron transport material that effectively extracts photo-generated electrons from perovskite layer. Similarly, the hole transport material facilitates efficient hole extraction, enhancing overall device performance. Moreover, the performance and durability of PSCs heavily rely on the composition, properties, and compatibility of these functional layers. A two-step simulation approach is used in this work. In the first step, various ETL and HTL materials were analysed in combination with the $(\text{NH}_4)_3\text{Sb}_2\text{I}_9$ absorber layer to identify the configuration yielding the highest performance. Once the optimal combination was determined, the second step focused on refining the selected model to enhance key performance factors, including PCE, J_{sc} , V_{oc} , and FF.

2.5 About the SCAPS-1D software

SCAPS-1D is a software tool created by Professor Marc Burgelman and used for simulation Work. It is a one-dimensional simulation tool that lets us build solar cell structures with up to seven layers, including absorber, ETL, HTL, and contacts. For each layer, we can define parameters like thickness, doping, mobility, band gap, and defect density. SCAPS simulates the device behaviour under different conditions and calculates key outputs like J-V, QE, C-V, and C-f curves. I used it to see how changes in parameters affect fill factor, V_{oc} , J_{sc} , and efficiency. There is also a feature of batch calculation tool that I used to vary parameters automatically and study their impact on performance, which helped in optimizing the device. SCAPS also has a scripting option, but I mainly used the graphical interface as it was enough for my work.

SCAPS-1D of version 3.3.11 can compute semiconductor equations for charge carriers by solving Poisson's and continuity equations. Software's core operation involves using the

Gummel-type iterative method and numerical differentiation to resolve the continuity and Poisson's derivative equations.

It uses semiconductor equations for charge carriers, such as continuity equation of hole (1), electron (2), and poison equation (3), and calculates performance of the solar devices [12]

$$\frac{dn_p}{dt} = G_n - \frac{n_p - n_{p^0}}{\tau_n} - n_p \mu_n \frac{dE}{dx} - \mu_n \xi \frac{dn_p}{dx} + D_n \frac{d^2 n_n}{dx^2} \quad (1)$$

$$\frac{dp_n}{dt} = G_p - \frac{p_n - p_{n^0}}{\tau_p} - p_n \mu_p \frac{dE}{dx} - \mu_p \xi \frac{dp_n}{dx} + D_p \frac{d^2 p_n}{dx^2} \quad (2)$$

$$\frac{d}{dx} \left(-\varepsilon(x) \frac{d\phi}{dx} \right) = q[p(x) - n(x) + N_d^+(x) - N_a^-(x) + p_t(x) - n_t(x)] \quad (3)$$

Where $p(x)$ and $n(x)$ represent concentration of free holes and concentration of free electrons respectively. $N_a^-(x)$, $N_d^+(x)$, $n_t(x)$, and $p_t(x)$, represent ionized acceptor concentration, ionized donor concentration, concentration of trapped electrons, and concentration of trapped hole, respectively. G , D , and ξ represent generation rate, diffusion coefficient, and electric potential, respectively. [12].

In addition, it is capable of evaluating spectral responses and current-voltage characteristics across a range of user-defined wavelengths. Notably, SCAPS-1D has the intrinsic ability to replicate both bulk and interface defects, making it widely utilized tool for numerical analysis of solar cells. The software incorporates the SRH recombination mechanism to accurately model charge carrier dynamics. Additionally, it supports standard illumination conditions of A.M 1.5G (Air Mass) and operating temperature at 300 K, ensuring reliable and consistent simulation results. Consequently, numerical analyses of PSC through SCAPS-1D represent a promising methodology for further advancing solar technology.

SCAPS-1D has some limitations like It neglects optical effects such as scattering and reflection and assumes zero reflection and full transmission, which leads to overestimated performance. It also does not consider degradation mechanisms such as ion migration or moisture sensitivity, which makes it unsuitable for stability analysis. Finally, its defect modelling is oversimplified, which fails to capture the complexity of the actual interface or bulk defects present in devices.

Chapter 3

Methodology

3.1 Overview: Procedure

In previous chapter we discussed about the SCAPS-1D software, now in this section describes the step-by-step procedure followed to simulate the solar cell structure in SCAPS-1D that helped in identifying the best-performing structure. To carry out the whole simulation process, the following steps are taken, as shown in fig. (3.1) There is also a detailed procedure for each step, which helps us in understand how we simulate cell models.

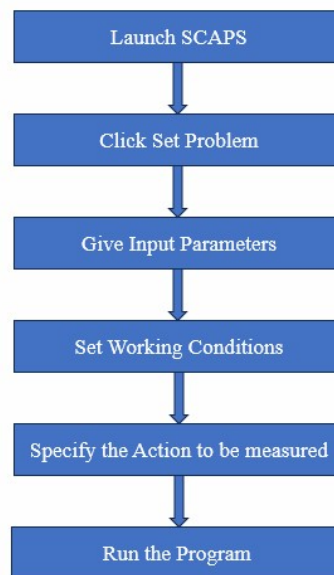
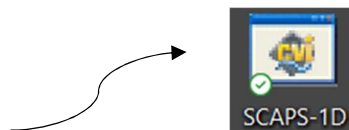
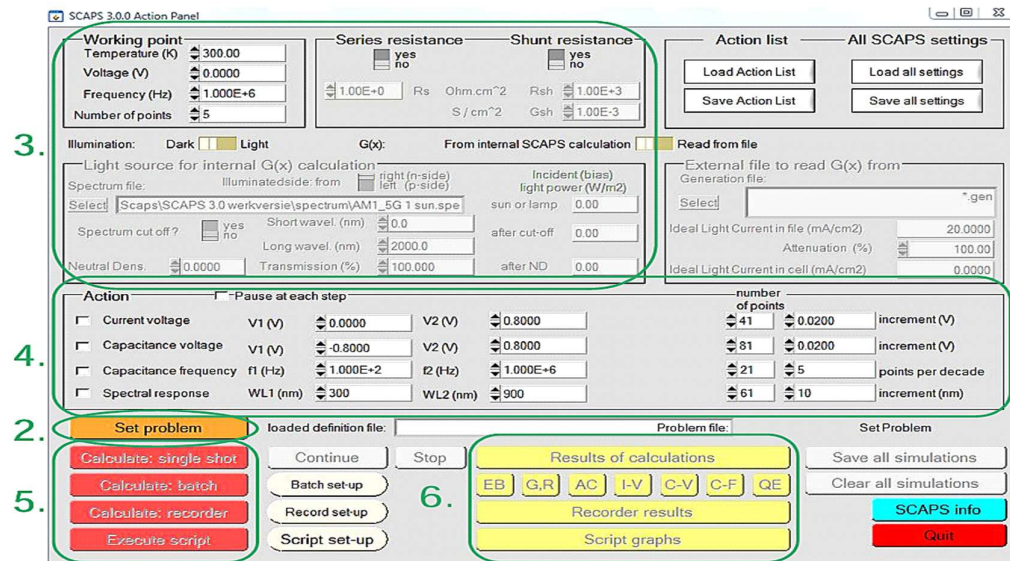


Fig. 3.1 Simulation Procedure.

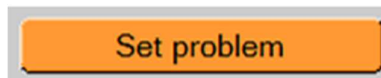
1: Run the SCAPS



This type of icon is shown on the desktop, click it, then a window opens showing Action Panel.



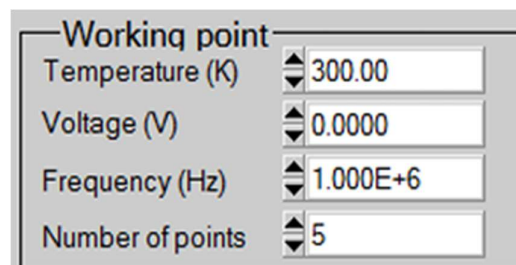
2. Set Problem;



In the action panel there is a button showing Set Problem, it is used to make the device structure.

3. Working Points;

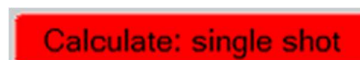
Working points are those parameters that do not change during the simulation process.



4. Select Measurement to simulate;

In this action panel I-V, C-V, C-f and QE(λ) are given, one can select according to their need, what they want to calculate. One can also adjust the number of steps in this panel.

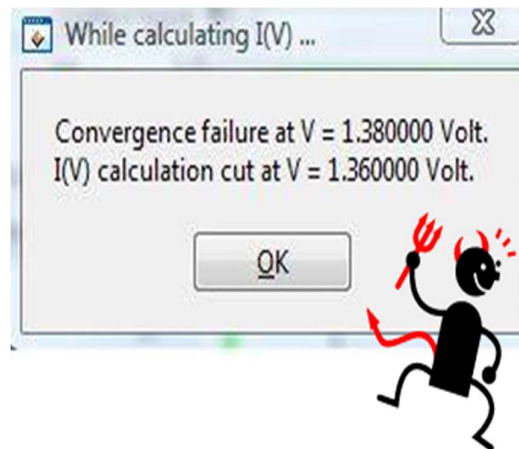
5. Start the calculation;



Once the whole parameters are set this button is used to start the calculation.

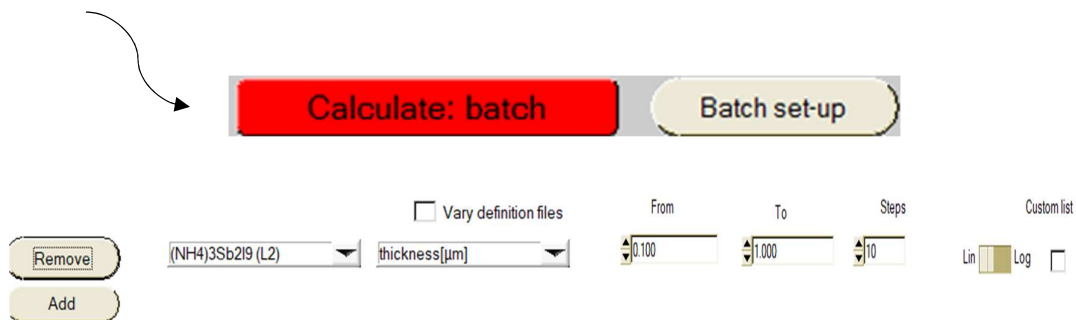
If the calculation result shows things like as shown in the image.

This is a convergence error, which means there is some issue in the data that we have fed during the simulation.



6. Batch Calculation;

To speed up simulation and if we want to study influence of a specific parameter, batch option in SCAPS is useful. By clicking on *Batch set-up*, we can open a panel that lets you select the parameter to vary and define its range. This allows us to observe how changes in that parameter influence the device characteristics.

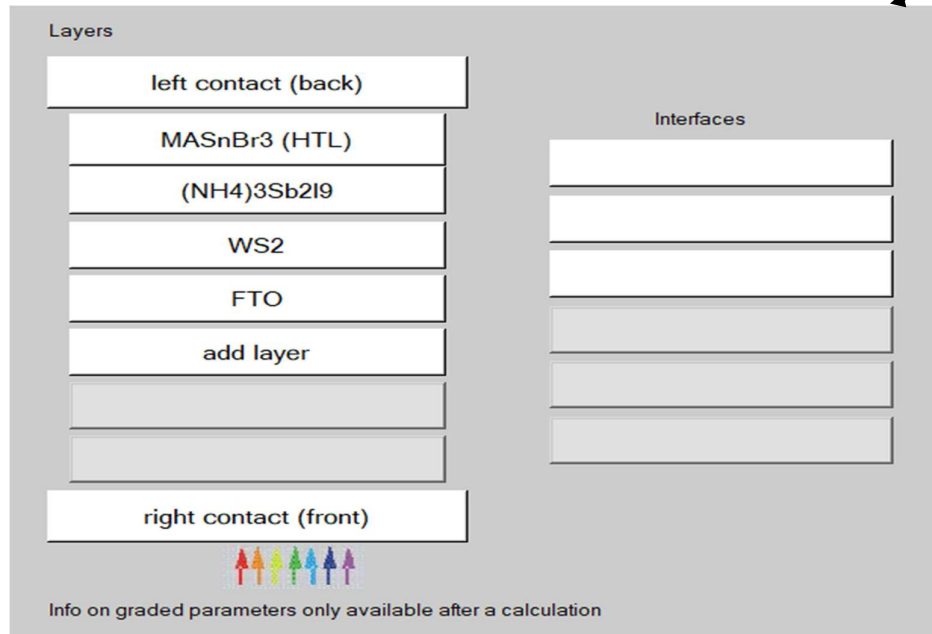


7. Solar cell definition panel;

It consists of *Add layers* button from which we feed the data of a given layer whether it is absorber or HTL or ETL. It looks like the below image.



It has a Layer panel that supports up to seven layers of different materials; for our modelling, we use different HTL, ETL and $(\text{NH}_4)_3\text{Sb}_2\text{I}_9$ as absorber material. It is shown in below image.



When we click on the layer, for example, the left contact (back), a different section opens where we can add the metalwork function of the back contact that is use in the PSC model as shown in below image.

Left Contact (Back)

Electrical properties

Thermionic emission / surface recombination velocity (cm/s):

electrons $1.00\text{E}+5$

holes $1.00\text{E}+7$

Metal work function (eV) 5.1000 or ☐ flat bands

Majority carrier barrier height (eV):

relative to EF 0.4400

relative to EV or EC 0.4400

☐ Allow contact tunneling

Effective mass of electrons $1.00\text{E}+0$

Effective mass of holes $1.00\text{E}+0$

Optical properties

optical filter ☐

Filter Mode ☒ transmission ☐ reflection

Filter Value 0.000000

Complement of Filter Value $1.0000\text{E}+0$

From Value ☐

From File ☐

Select Filter File

OK cancel

For the materials properties, click on the next layer, and again, a section will open as shown in the image below. These are the required properties needed for the simulation. We need to review papers to find them.

SCAPS 3.3.11 Layer Properties Panel

LAYER 2 (NH4)3Sb2I9

thickness (μm) 0.500

uniform pure A ($y=0$) 0.000

The layer is pure A: $y = 0$, uniform

Semiconductor Property P of the pure material pure A ($y = 0$)

bandgap (eV) 2.050

electron affinity (eV) 3.800

dielectric permittivity (relative) 7.000

CB effective density of states ($1/\text{cm}^3$) $1.000\text{E}+19$

VB effective density of states ($1/\text{cm}^3$) $1.000\text{E}+19$

electron thermal velocity (cm/s) $1.000\text{E}+7$

hole thermal velocity (cm/s) $1.000\text{E}+7$

electron mobility (cm^2/Vs) $1.230\text{E}+1$

hole mobility (cm^2/Vs) $4.800\text{E}+0$

☐ Allow Tunneling

effective mass of electrons $1.000\text{E}+0$

effective mass of holes $1.000\text{E}+0$

no ND grading (uniform)

shallow uniform donor density ND ($1/\text{cm}^3$) $0.000\text{E}+0$

no NA grading (uniform)

shallow uniform acceptor density NA ($1/\text{cm}^3$) $0.000\text{E}+0$

We can also add defect properties of materials that are used in this modelling. Once the data is fed, just click on accept button, and that's all.

In the solar cell definition panel, on the right-hand side, *accept* buttons are there; once the data is fed, just click on the accept button, and we come to the action panel where we just click on the *Calculate: single shot*, and that's all. Now we are ready for the result of our simulation. This is the whole procedure of the simulation.

3.2 Device Structure and Simulation

The device having structure FTO/ETL/absorber layer/HTL/Back Contact is used for the simulation work, where $(\text{NH}_4)_3\text{Sb}_2\text{I}_9$ is absorber layer and Au is Back contact having work function 5.1 eV. We simulated the given model with different HTLs and ETLs combinations and selected the model with the highest device performance parameter. The ETLs used in this work include WS_2 , IGZO, TiO_2 , and PCBM, whereas PEDOT, ZnTe, spiro-OMeTAD, and MASnBr_3 are HTLs. The device model and band alignment diagram for the $(\text{NH}_4)_3\text{Sb}_2\text{I}_9$ -based PSC are shown in fig. (3.2), as this structure is selected for further optimization. The values of material properties for FTO (fluorine-doped tin oxide), HTL, and ETLs are displayed in Tables (3.1), (3.2) and (3.3), along with their respective references. For absorber layer $(\text{NH}_4)_3\text{Sb}_2\text{I}_9$, the simulation parameters were obtained from previous literature [10], [13], [14]. The band gap (E_g) of $(\text{NH}_4)_3\text{Sb}_2\text{I}_9$ is 2.05 eV. The value of the dielectric constant is 7. The mobility of holes (μ_p) and electrons (μ_n) are 4.8 and $12.3(\text{cm}^2/\text{Vs})$, respectively. The thermal velocity of both holes and electrons is $1 \times 10^7(\text{cm/s})$ each, as used in this work.

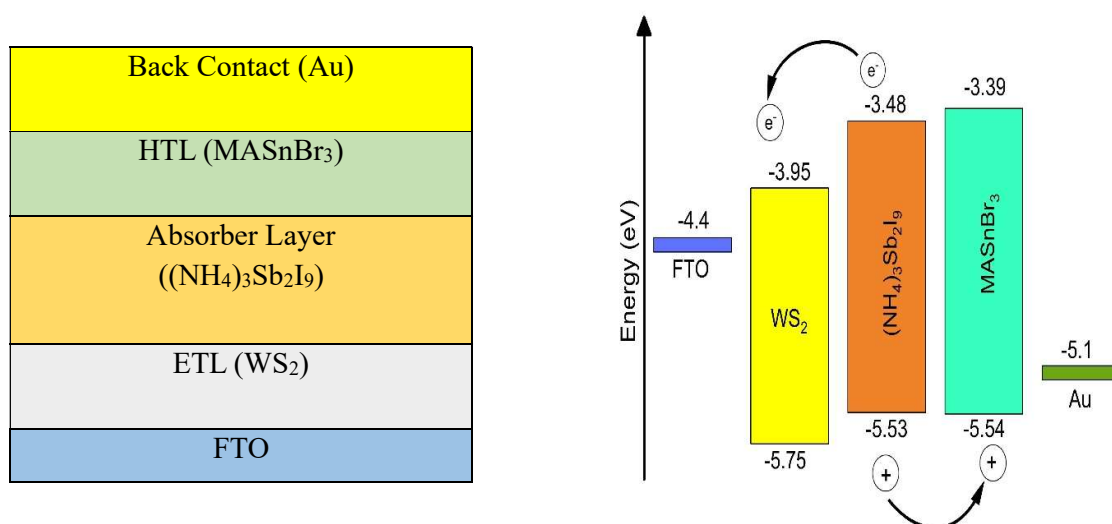


Fig. 3.2 Device Structure and energy band diagram for $(\text{NH}_4)_3\text{Sb}_2\text{I}_9$ -based PSC.

Table 3.1. Initial input parameter of PSC.

Parameter	FTO	TiO ₂	(NH ₄) ₃ Sb ₂ I ₉	Spiro-OMeTAD
Thickness (nm)	50	100	500	100
E _g (eV)	3.5	3.2	2.05	3.0
χ (eV)	4.0	4	3.8*	2.45
ϵ_r	9.0	9	7.0*	3.0
N _c (cm ⁻³)	2.2×10^{18}	10^{21}	1×10^{19}	1×10^{19}
N _v (cm ⁻³)	1.8×10^{19}	2×10^{20}	1×10^{19}	1×10^{19}
μ_n (cm ² /Vs)	20	20	12.3	1×10^{-4}
μ_p (cm ² /Vs)	10	10	4.8	1×10^{-4}
N _D (cm ⁻³)	1×10^{15}	10^{19}	0	0
N _A (cm ⁻³)	0	4×10^{15}	0	2×10^{18}
N _t (cm ⁻³)	1×10^{15}	1×10^{13}	1×10^{13}	1×10^{14}
References	[15], [16]	[17]	[10], [14]	[18], [19], [20], [21]

*In this work.

Table 3.2. Parameters for simulation of different HTLs.

Parameter	ZnTe	PEDOT: PSS	Spiro-OMeTAD	MASnBr ₃
Thickness (nm)	100	100	100	100
E _g (eV)	2.26	2.2	3.0	2.15
χ (eV)	3.65	2.9	2.45	3.39
ϵ	14.0	3.0	3.0	8.2
N _C (cm ⁻³)	7.5×10^{17}	2.2×10^{15}	1×10^{19}	1×10^{18}
N _V (cm ⁻³)	1.5×10^{19}	1.8×10^{18}	1×10^{19}	1×10^{18}
μ_n (cm ² /Vs)	70	1×10^{-2}	1×10^{-4}	1.6
μ_p (cm ² /Vs)	50	2×10^{-4}	1×10^{-4}	1.6
N _D (cm ⁻³)	0	0	0	0
N _A (cm ⁻³)	2.16×10^{19}	1×10^{19} *	2×10^{18}	1.0×10^{18}
N _t (cm ⁻³)	1×10^{14}	1×10^{14}	1×10^{14}	1×10^{14}
References	[22], [23]	[24]	[18], [19], [20], [21]	[25], [26]

* In this work.

Table 3.3 Parameters for simulation of different ETLs.

Parameters	TiO ₂	IGZO	WS ₂	PCBM
Thickness(nm)	50	50	100	100
E _g (eV)	3.2	3.05	1.8	2.1
χ (eV)	4	4.16	3.95	3.9
ε _r	9	10	13.6	7.0
N _c (cm ⁻³)	10 ²¹	5×10 ¹⁸	1 ×10 ¹⁸	2.2 x10 ¹⁹
N _v (cm ⁻³)	2×10 ²⁰	5×10 ¹⁸	2.4 ×10 ²⁰	2.2 x 10 ¹⁹
μ _e (cm ² V ⁻¹ s ⁻¹)	20	15	100	0.001
μ _h (cm ² V ⁻¹ s ⁻¹)	10	0.1	100	0.002
V _c (cm ² s ⁻¹)	1.0×10 ⁷	1.0×10 ⁷	1.0×10 ⁷	1.0×10 ⁷
V _h (cm ² s ⁻¹)	1.0×10 ⁷	1.0×10 ⁷	1.0×10 ⁷	1.0×10 ⁷
N _D (cm ⁻³)	10 ¹⁹	1.0×10 ¹⁸	1 ×10 ¹⁸	1 x 10 ¹⁸
N _A (cm ⁻³)	4×10 ¹⁵	0	0	0
N _t (cm ⁻³)	10 ¹⁵	1.0×10 ¹⁴	1.0×10 ¹³	1.0×10 ¹⁴
References	[17]	[27]	[28]	[29]

Table 3.4. Various Device Structures and their simulation results.

Device Structures	V _{oc} (V)	J _{sc} (mA/cm ²)	FF (%)	PCE (%)
FTO/WS ₂ /(NH ₄) ₃ Sb ₂ I ₉ /MASnBr ₃ /Au	1.65	13.37	88.40	19.51
FTO/WS ₂ /(NH ₄) ₃ Sb ₂ I ₉ /spiro-OMeTAD/Au	1.65	13.29	82.56	18.12
FTO/WS ₂ /(NH ₄) ₃ Sb ₂ I ₉ /ZnTe/Au	1.53	13.34	81.24	16.63
FTO/WS ₂ /(NH ₄) ₃ Sb ₂ I ₉ /PEDOT: PSS/Au	1.65	13.36	76.92	16.98
FTO/PCBM/(NH ₄) ₃ Sb ₂ I ₉ /ZnTe/Au	1.61	11.30	79.50	14.48
FTO/PCBM/(NH ₄) ₃ Sb ₂ I ₉ /spiro-OMeTAD/Au	1.74	11.24	80.64	15.83
FTO/PCBM/(NH ₄) ₃ Sb ₂ I ₉ /MASnBr ₃ /Au	1.73	9.92	85.53	14.74
FTO/PCBM/(NH ₄) ₃ Sb ₂ I ₉ /PEDOT: PSS/Au	1.74	11.32	78.81	15.59
FTO/TiO ₂ /(NH ₄) ₃ Sb ₂ I ₉ /ZnTe/Au	1.60	11.25	80.04	14.46
FTO/TiO ₂ /(NH ₄) ₃ Sb ₂ I ₉ /spiro-OMeTAD/Au	1.74	11.156	80.78	15.75
FTO/TiO ₂ /(NH ₄) ₃ Sb ₂ I ₉ / MASnBr ₃ /Au	1.74	11.29	85.58	16.89
FTO/TiO ₂ /(NH ₄) ₃ Sb ₂ I ₉ /PEDOT: PSS/Au	1.97	7.92	69.39	10.86
FTO/IGZO/(NH ₄) ₃ Sb ₂ I ₉ /ZnTe/Au	1.60	11.26	80.11	14.49
FTO/IGZO/(NH ₄) ₃ Sb ₂ I ₉ /spiro-OMeTAD/Au	1.74	11.16	80.86	15.78
FTO/IGZO/(NH ₄) ₃ Sb ₂ I ₉ / MASnBr ₃ /Au	1.74	11.30	85.66	16.92
FTO/IGZO/(NH ₄) ₃ Sb ₂ I ₉ /PEDOT: PSS/Au	1.74	11.29	79.30	15.66

Chapter 4

Results and discussion

4.1. Optimization of Appropriate ETL and HTL

HTL and ETL are essential components in ensuring efficient charge carrier movement within a solar cell. They seamlessly transport charge carriers, which is vital for minimizing charge recombination, otherwise reducing device performance. In our study, we explored four HTLs-ZnTe, PEDOT: PSS, MaSnBr_3 , and Spiro-OMeTAD, and four ETLs- WS_2 , IGZO, PCBM, and TiO_2 . Energy band diagram of absorber layer with different HTLs and ETLs shown below in fig. (4.1). The Impact of distinct HTLs such as MASnBr_3 , PEDOT: PSS, ZnTe, and Spiro-OMeTAD were studied with different combinations. ZnTe, and PEDOT: PSS shows less efficiency than other HTLs. Band matching is a vital factor to achieve maximum performance of the device. WS_2 , as ETL, has conduction band minimum (CBM) of -3.95 eV lower than the absorber's CBM (-3.48 eV), enabling smooth electron extraction. Its deep valence band (-5.75 eV) blocks hole leakage, and its high electron mobility (~ 100 $\text{cm}^2/\text{V}\cdot\text{s}$) ensures fast charge transport with low resistive losses outperforming traditional ETLs like TiO_2 . On the flip side, MASnBr_3 as the HTL aligns perfectly with the absorber's conduction band minimum (VBM) of -5.53 eV, so holes can flow smoothly into MASnBr_3 without barriers. Its CBM (-3.39 eV) is higher than the absorber's CBM, which effectively blocks any electron flow in the wrong direction. This ensures that MASnBr_3 not only transports holes efficiently but also prevents electron recombination. The valence band maximum should align well with VBM of absorber layer to allow efficient hole extraction. Conduction band maximum should be higher than CBM of absorber layer to block electron transport, which helps reduction in recombination and increase open circuit voltage of PSC. Also, MASnBr_3 is most appropriate HTL as it has better stability than Spiro-OMeTAD or PEDOT: PSS can provide, suitable for flexible devices or tandem cells, efficient hole extraction and minimizes energy loss, environmentally friendly and low-cost. The MASnBr_3 as the HTL gave the best band alignment compared to the other HTLs shown in fig. (4.1). Their effect on performance variables of PSCs was evaluated using SCAPS-1D simulations. The choice of these specific HTLs and ETLs was guided by their strong performance, as reported in earlier

studies, demonstrating their potential to enhance PCE and their suitability for integration into PSC designs. The simulation parameters for each HTL and ETL are detailed in Tables 3.2 and 3.3. A decline in Q.E. is often linked to factors such as reduced absorption at longer wavelengths and surface recombination [31]. Fig. (4.2) shows the J-V and Q.E. plots, illustrating these effects. Table 3.4 represents simulation results of all the combinations of ETLs and HTLs with an absorber layer. The outcomes deduced WS_2 along with MASnBr_3 show the highest PCE.

WS_2 ETL-based PCS configuration shows better PCE due to higher carrier mobility, which enables faster charge transport and reduces recombination losses, and band alignment balances efficiency by maximizing sunlight absorption while minimising voltage losses [30]. MASnBr_3 , used as the HTL, demonstrated highest efficiency of 19.51 % when paired with WS_2 . Based on this performance, MASnBr_3 was selected as the HTL for optimizing the absorber layer parameters. This thin-film material offers a tunable bandgap and excellent light absorption properties. However, the presence of Sn^{2+} in MASnBr_3 poses challenges due to its instability and susceptibility to oxidation, which degrade the film's morphology and semiconductor properties, ultimately lowering efficiency and stability [31], [32]. Fortunately, methods to prevent oxidation of Sn^{2+} and enhance stability of the material have been proposed [33]. As a result, in the subsequent sections of our study, the device structure $\text{FTO}/\text{WS}_2/(\text{NH}_4)_3\text{Sb}_2\text{I}_9/\text{MASnBr}_3/\text{Au}$ was chosen for further optimization. Factors such as thickness, temperature, and defect density were investigated to improve device's performance.

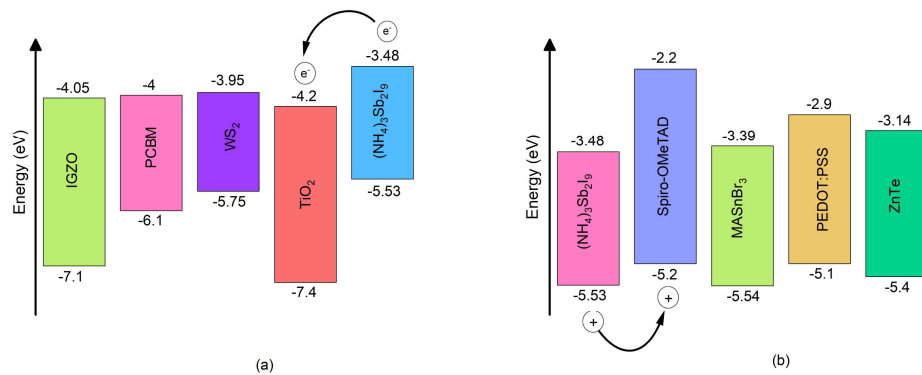


Fig. 4.1 Energy band diagram of absorber layer with different (a) HTLs and (b) ETLs.

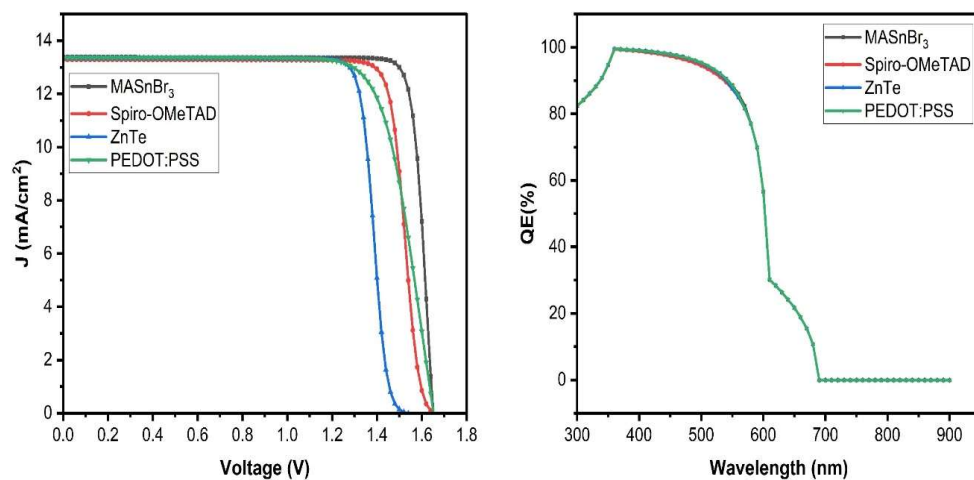


Fig. 4.2 J-V and QE characteristics of distinct HTLs with WS_2 as ETL.

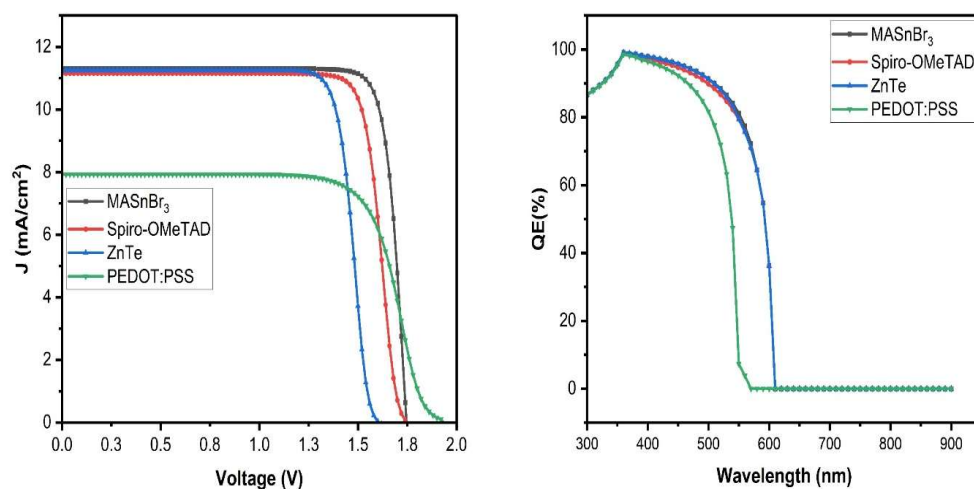


Fig. 4.3 J-V and QE characteristics of distinct HTLs with TiO_2 as ETL.

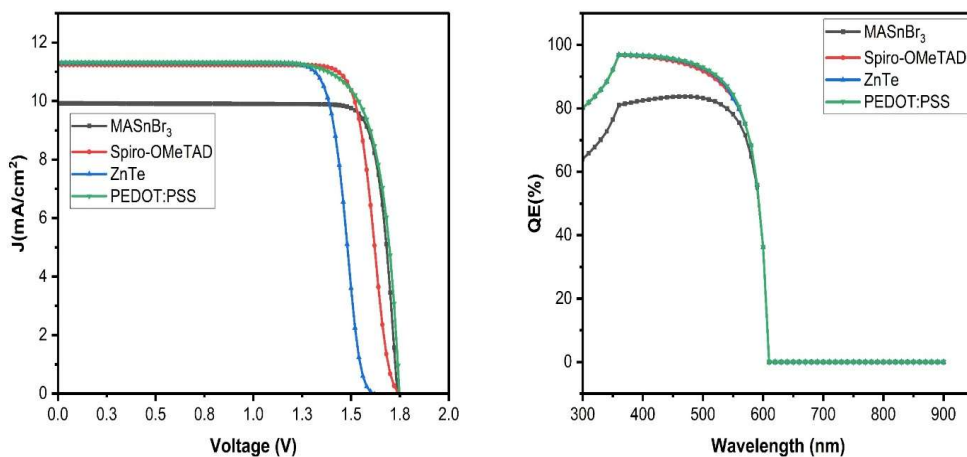


Fig. 4.4 J-V and QE characteristics of distinct HTLs with PCBM as ETL.

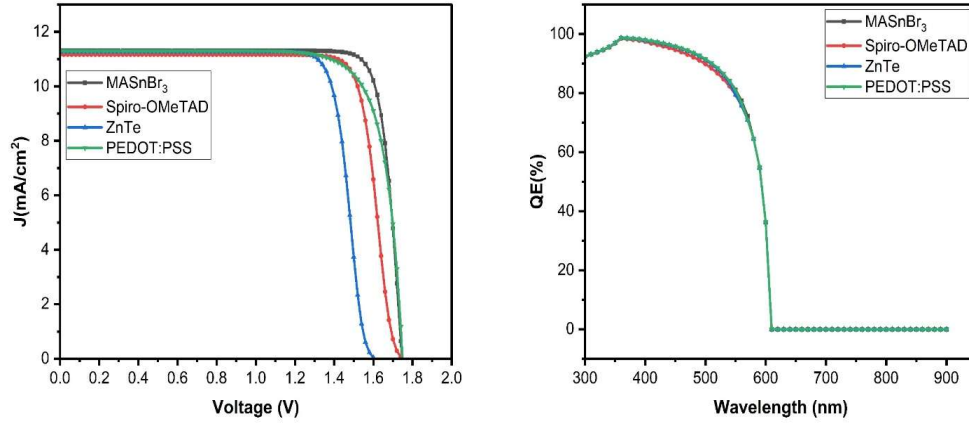


Fig. 4.5 J-V and QE characteristics of distinct HTLs with IGZO as ETL.

4.2 Impact of defect density

Simulations were conducted through batch calculation varying N_t from 10^{13} to 10^{18} cm^{-3} to evaluate impact of N_t of $(\text{NH}_4)_3\text{Sb}_2\text{I}_9$. Defects were considered both at the surface and within the bulk of the $(\text{NH}_4)_3\text{Sb}_2\text{I}_9$ layers. In perovskite materials, several types of point defects can arise, including interstitial defects, lattice vacancies, as well as Schottky and Frenkel defects. Moreover, structural imperfections such as dislocations and grain boundaries significantly assist in overall defect density [34]. These defects introduce additional energy states within the bandgap, which serve as traps for charge carriers [35], affecting the device's efficiency and performance. We varied N_t of absorber layer in step 10^1 , keeping its thickness at 500 nm. Other material parameters were kept the same, as given in Table (1). Impact of N_t on device's performance is displayed in fig. (4.6), which reveals that an increase in N_t causes a considerable drop in performance parameters. At $N_t = 10^{13} \text{ cm}^{-3}$, the efficiency of PCS is 19.51 % and 18.94 % at $N_t = 10^{14} \text{ cm}^{-3}$; above this value, the PCE decreases continuously, and it comes to 1.59 % at $N_t = 10^{18} \text{ cm}^{-3}$. Optimized value of N_t is 10^{13} cm^{-3} [36] for further simulation work as it gives the highest performance parameters. N_t is crucial in determining the recombination rate within a solar cell, which can be effectively explained through the SRH recombination model. This model comprehensively describes the recombination process and is mathematically represented by eq (4) [37].

$$R = \frac{\tau_{n,p}^{-1}(np - n_i^2)}{n + p + 2n_i \coth\left(\frac{E_t - E_i}{KT}\right)} \quad (4)$$

where $\tau_{n,p}$, n , p , represent charge carrier lifetime, electron density, and hole density, respectively. n_i is intrinsic density, E_t is energy level of trap defects and E_i is intrinsic energy levels. The lifetime of the charge carrier can be calculated by eq. (5) [37].

$$\tau_{n,p} = \frac{1}{\sigma_{n,p} v_{th} N_t} \quad (5)$$

where N_t represent defect density of the absorber layer, $\sigma_{n,p}$ is capture cross-section of charge carriers and v_{th} is velocity of charge carriers. Charge carrier lifetime and defect density are closely related in an inverse manner, as outlined in eq (5). Moreover, there is an inverse relationship between R and $\tau_{n,p}$ of charge carriers, as illustrated in eq (4). Therefore, as defect density increases, recombination rate also rises due to drop in $\tau_{n,p}$ and diffusion length. This reduces the total performance of PSC.

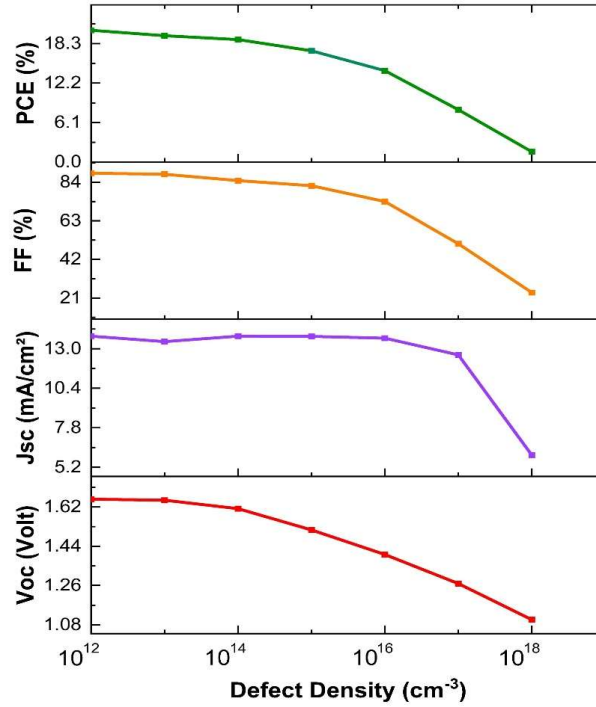


Fig. 4.6 The impact of defect density on performance parameters of PSC.

4.3 Impact of thickness

The impact of the absorber layer thickness on PSC performance was explored by adjusting its thickness from 100 nm to 1000 nm while keeping constant values for other parameters. As shown in fig. (4.7), results indicate that increasing thickness leads to improved efficiency. This is because at smaller thicknesses, photons are not absorbed efficiently. However, V_{oc} dropped from 1.6672 V to 1.5225 V due to a rise in charge carriers' recombination over longer travel paths [38]. The J_{sc} rises sharply with thickness up to 400 nm, then gradually increases beyond 500 nm. The higher J_{sc} (14.16 mA/cm²) observed at 1000 nm is primarily due to high absorption coefficient of absorber material. While FF decreased from 89.31 to 87.36 %, likely due to increased series resistance, enhanced charge carrier recombination, and associated resistive losses. [39]. As efficiency does not change much after 700 nm, so we took 700 nm as optimal thickness for device structure.

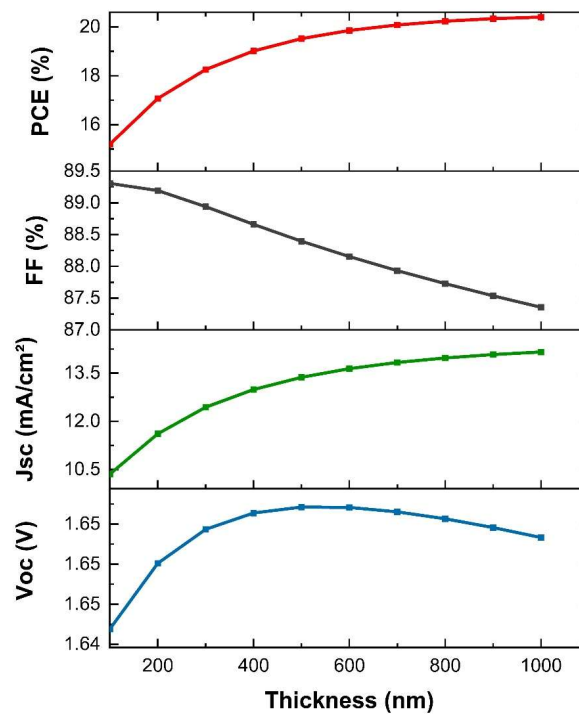


Fig. 4.7. Impact of thickness of Absorber layer on performance parameters.

4.4 Impact of operating temperature on device performance

The performance of device is significantly influenced by temperature as it impacts its efficiency and stability. While standard operating temperature is typically set at 300 K, real-world applications expose devices to a broad temperature range, compromising the device structure and degrading its performance. To assess the effect of temperature on four key parameters of PSC and evaluate its thermal stability, temperatures were varied from 280 K to 420 K. Impact of this temperature variation on performance metrics is shown in Fig (4.8). The analysis indicated a decline in PCE, V_{oc} and FF, on other hand J_{sc} showed a slight increase. This behaviour is due to the increased strain and stress induced by rising temperatures, which lead to greater interfacial defects, structural disorder, and reduced layer connectivity [40]. Higher temperatures also affect the mobilities of charge carriers, as well as carrier concentration, which collectively reduces the efficiency of PSCs. Drop in V_{oc} with temperature is primarily because of rise in J_0 , as given by eq. (6).

$$V_{oc} = \frac{KT}{q} \left(\frac{J_{sc}}{J_0} + 1 \right) \quad (6)$$

where J_{sc} and J_0 represent short circuit and reverse saturation current, respectively. K is Boltzmann constant and T is temperature in kelvin. Meanwhile, a small increase in J_{sc} is due to a narrowing of semiconductor's band gap at higher temperatures, enabling the absorption of longer-wavelength photons.

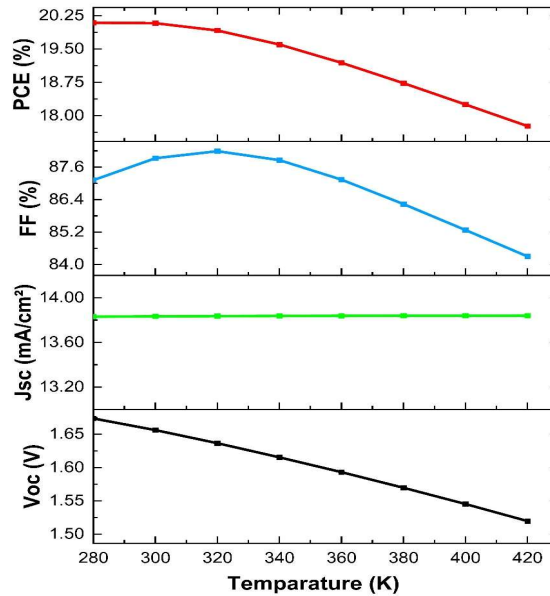


Fig. 4.8 Impact of Temperature on $(NH_4)_3Sb_2I_9$ -based PSC.

4.5 Impact of Doner Density

N_d varied from 10^{12} to 10^{18} cm^{-3} , and its consequences on PCE and FF is highlighted in fig. (4.9). From the plot, it is seen that PCE remains at 20.08% from 10^{12} to 10^{15} cm^{-3} ; after that, it started decreasing to 8.77% at 10^{18} cm^{-3} . FF also remains at 87.9322 % from 10^{12} to 10^{14} , then slightly increases and starts decreasing to 86.68 % at 10^{18} cm^{-3} . The reason behind this may include the recombination factor that reduces PCE and FF at higher N_d .

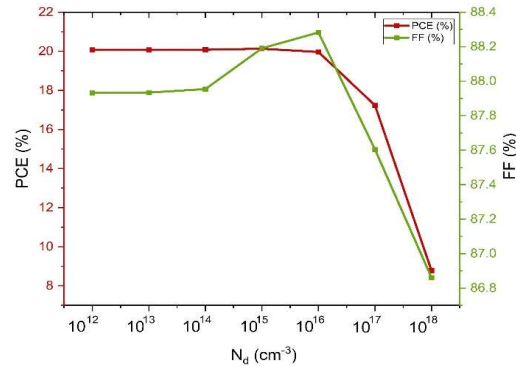


Fig. 4.9 Impact of acceptor density on $(\text{NH}_4)_3\text{Sb}_2\text{I}_9$ -based PSC

4.6 Impact of Series and Shunt Resistance

The consequences of series (R_s) and shunt (R_{sh}) resistance are demonstrated in Fig. (4.10). Fig. 4.10 (a) shows that increasing R_s from 0 to $6 \Omega\text{-cm}^2$ at fixed $R_{sh} = 10^5 \Omega\text{-cm}^2$ leads to a slight decline in PCE from 20.05 % at $0 \Omega\text{-cm}^2$ to 18.97 % at $6 \Omega\text{-cm}^2$ and FF from 87.84 % to 83.09 at 0 and $6 \Omega\text{-cm}^2$ respectively, due to voltage drops across the cell layers, while J_{sc} and V_{oc} remain relatively unaffected. The PSC has high performance at minimum series resistance. This highlights the importance of minimizing R_s through optimized layer deposition, improved contacts, and reduced cell dimensions [41].

Conversely, Fig. 4.10 (b) displays that increasing R_{sh} from 10^1 to $10^6 \Omega\text{-cm}^2$ at fixed series resistance $R_s = 0.5 \Omega\text{-cm}^2$ enhances PCE, FF, J_{sc} , and V_{oc} . The substantial increase in PCE from 0.45 to 19.98% suggests a notable improvement in charge carrier generation and collection efficiency, likely resulting from enhancements in the device's structural design [42]. FF rapidly increases from 24.99 to 78.6 % and then gradually increases to 87.53 %. Similarly, V_{oc} suddenly changes from 0.13 to 1.37 V and then becomes flat to 1.65 V, and J_{sc} changes from 13.17 to 13.76, and then it also becomes flat at 13.83 mA. So, achieving

high PSC performance requires low R_s to minimize resistive losses and high R_{sh} to prevent leakage currents.

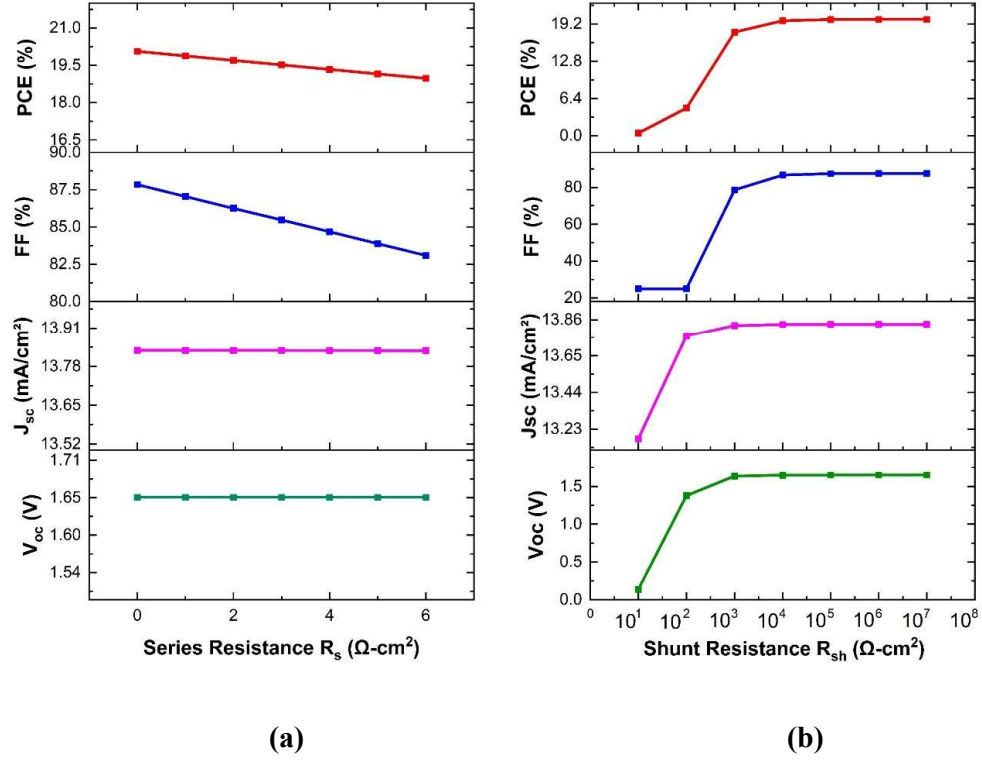


Fig.4.10 Impact of (a) R_s at $R_{sh} = 10^5 \text{ (}\Omega\text{-cm}^2\text{)}$ and (b) R_{sh} at $R_s = 0.5 \text{ (}\Omega\text{-cm}^2\text{)}$ on performance parameter of PSC

4.7 Impact of back contact on PSC

The work function of electrode significantly impacts device's performance. The simulation was performed to investigate influence of the back electrode on device parameters. Work function of different contact is tabulated in Table 4.1. Fig. 4.11 (a-b) shows the energy bands of device structure FTO/WS₂/(NH₄)₃Sb₂I₉/MASnBr₃ with different electrodes. Fig. 4.11 (a), demonstrated that electrodes with lower work functions, such as carbon (C), gold (Au), and nickel (Ni), form a Schottky barrier at the interface of HTL/electrode, pointed by dashed oval shaped frame. This barrier obstructs hole transfer, resulting in decreased PCE and FF, as shown in fig. 4.11 (b). In contrast, platinum (Pt) creates an ohmic contact at the HTL/Pt interface [43]. This ohmic contact facilitates smoother hole transfer, enabling Pt to achieve better PCE than other contacts, illustrated in fig. 4.12 (b). The influence of

various back contacts on the J-V characteristics is highlighted in fig. 4.12 (a). The barrier potential at the anode/MASnBr₃ interface can be determined by eq. (7)

$$\varphi_B = \frac{E_g}{q} + \chi - \varphi_M \quad (7)$$

where E_g is band gap of MASnBr₃, χ is electron affinity of MASnBr₃ and φ_M is a rear metalwork function. As electrode work function decreases, the potential barrier at anode/MASnBr₃ interface rises. This increase in the barrier hampers charge transport, resulting in a decrement in both PCE and FF.

Table 4.1. Work Function of different electrode.

Back Contacts	C	Au	Ni	Pt
Work Function (eV)	5	5.1	5.5	5.7
PCE (%)	18.82	20.08	20.60	20.66

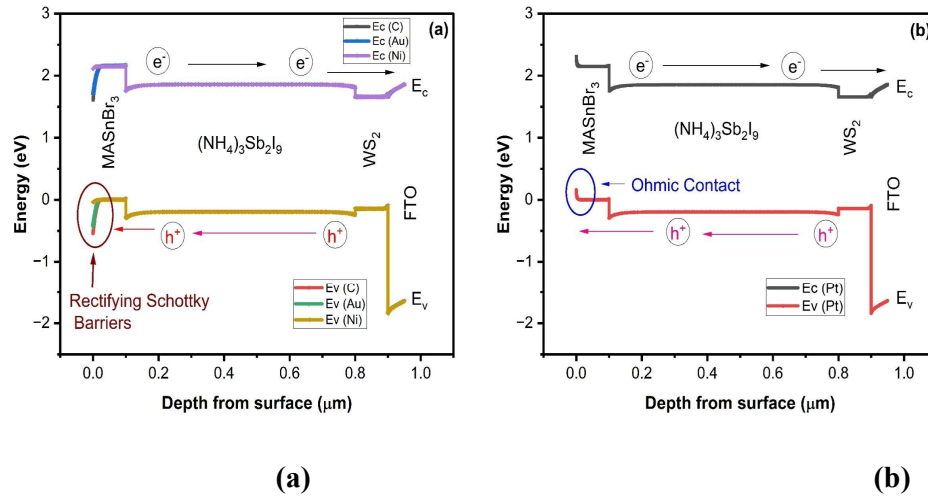


Fig. 4.11 Band gap energy of PSC vs distinct back contact. (a) C, Au, Ni (b) Pt.

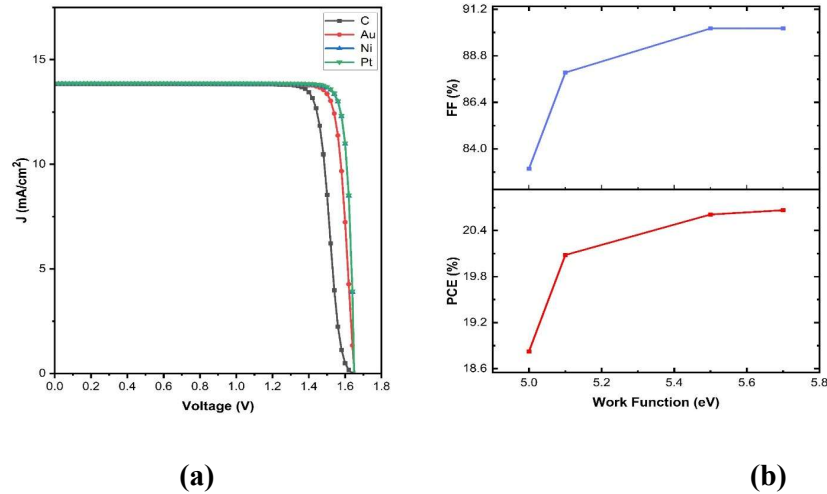


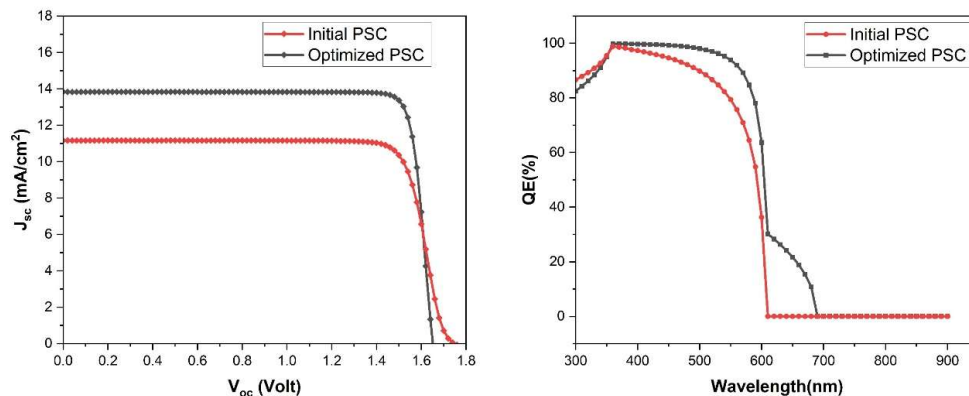
Fig. 4.12. (a) J-V of the device for distinct back contact. (b) PCE and FF for distinct back contact.

4.8 Comparison with Previous Reported Results

Table 4.2. shows comparison between initial PSC FTO/TiO₂/(NH₄)₃Sb₂I₉/spiro-OMeTAD/Au and optimized PSC FTO/WS₂/(NH₄)₃Sb₂I₉/MASnBr₃/Au and their J-V and QE characteristics are highlighted in Fig. (4.13). Organic spiro-OMeTAD is widely favoured due to its simple and adaptable production process, making it a popular choice in both commercial and industrial applications [43]. However, it faces significant drawbacks for use in PSCs, including low hole mobility, poor conductivity, high production costs, and vulnerability to moisture, oxidation, and light, which compromise its stability. Similarly, TiO₂ is well-established n-type material, frequently deployed as ETL. While it holds promise for excellent photovoltaic performance, challenges arise from its susceptibility to photo-corrosion, high thermal stability, and a wide bandgap of 3.2 eV [44]. Although PSCs using these materials alongside lead-based perovskites often exhibit superior characteristics, as evident from the data in the table, their toxicity and instability necessitate further research to identify safer and more stable alternatives. The comparison with previously reported result shown below Table 4.3 Therefore, this work's designed model can be considered for further experimentation and commercialization.

Table 4.2. Comparison of Initial and Optimized Device Structure.

Parameters	Initial PSC	Optimised PSC
V_{oc} (V)	1.74	1.65
J_{sc} (mA/cm ²)	11.15	13.83
FF (%)	80.78	87.93
PCE (%)	15.75	20.08

**Fig. 4.13 J-V and QE curve for initial and optimized PSC**

The band alignment and resulting band offsets (spike or cliff) between the absorber and ETL is crucial in explaining charge transport efficiency and recombination dynamics in planar PSC structure. The band alignment diagram of the optimized device, shown in Fig. (4.14) below, shows how charge carriers move across the device. Electrons naturally move from higher to lower energy levels, starting from $(\text{NH}_4)_3\text{Sb}_2\text{I}_9$ (with $E_C \sim$ ranging from 1.69 to 0.15 eV), then WS_2 ($E_C \sim 0.003$ eV), and finally to FTO ($E_C \sim 0.19$ eV). Similarly, the valence band alignment supports hole transport, allowing holes to move smoothly from $(\text{NH}_4)_3\text{Sb}_2\text{I}_9$ ($E_V \sim$ ranging from - 1.89 to -0.35 eV), and finally to MASnBr_3 ($E_V \sim -0.04$ eV). The CBO of -0.15 eV forms a small cliff at the $\text{WS}_2/(\text{NH}_4)_3\text{Sb}_2\text{I}_9$ interface. While negative CBO can lead to electron accumulation and interface recombination, this offset is small enough, so it allows efficient electron extraction without significant losses. Additionally, the high electron mobility of WS_2 has high electron mobility of $100 \text{ cm}^2/\text{V}\cdot\text{s}$ that ensures fast charge transport, reducing accumulation at the interface. While mobility doesn't eliminate the cliff, it only helps the system tolerate it, maintaining good device performance. The VBO between $(\text{NH}_4)_3\text{Sb}_2\text{I}_9/\text{MASnBr}_3$ is -0.31 eV, which makes the hole extraction efficient without interface recombination.

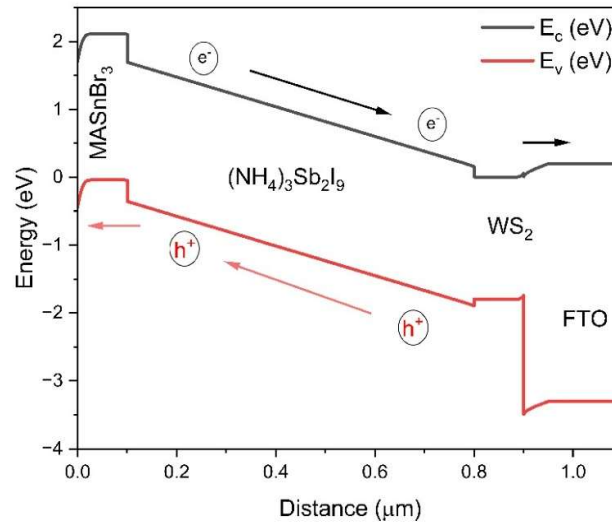


Fig. 4.14 Band offsets (Spike, Cliff) diagram of optimised device.

The fig. (4.15) shown below depicts the absorption coefficient plot of WS₂, PCBM, MASnBr₃, and (NH₄)₃Sb₂I₉. The WS₂ and PCBM layer overlapping in the absorption curves with absorber layer, it's important to note that they are used as thin layers. So, despite the similar absorption coefficients, their actual photon absorption is minimal. Most of the light still reaches the (NH₄)₃Sb₂I₉ perovskite layer, and photon loss through WS₂ or PCBM is practically negligible. This justifies their use as front ETL in planar structures, especially given their excellent band alignment and charge extraction capabilities.

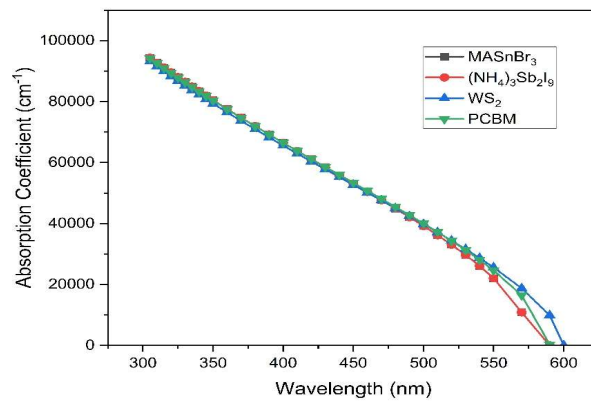


Fig. 4.15. Absorption coefficient plot of WS₂, PCBM, MASnBr₃, and (NH₄)₃Sb₂I₉ layers.

Table 4.3. Comparison with the previously reported work.

Device Structure	Work	V _{oc} (V)	J _{sc} (mA/cm ²)	FF (%)	PCE (%)	Reference
FTO/TiO ₂ /Cs ₃ Sb ₂ I ₉ /spiro-OMeTAD/Au	Simulation	1.32	13.13	72.01	12.54	[45]
FTO/TiO ₂ /Cs ₃ Sb ₂ I ₉ /NiO	Simulation	0.92	22.07	68.21	13.82	[46]
FTO/TiO ₂ /MA ₃ Sb ₂ I ₉ /Spiro-OMeTAD/Au	Simulation	1.41	12.49	84.00	14.90	[47]
FTO/TiO ₂ /(NH ₄) ₃ Sb ₂ I ₉ /Spiro-OMeTAD/Au	Experimental	0.945	1.16	42.00	0.42	[10]
FTO/WS ₂ /(NH ₄) ₃ Sb ₂ I ₉ /MASnBr ₃ /Au	Simulation	1.65	13.83	87.93	20.08	[Present work]

4.9 Feasibility of fabricating the proposed structure and strategies to improve PSCs

Performance Fabricating the FTO/WS₂/(NH₄)₃Sb₂I₉/MASnBr₃/Au proposed structure is feasible, but it presents several challenges that need to be addressed for high-performance and scalable solar cells. The interfaces between WS₂, the perovskites, and the gold electrode need optimization for charge transport and minimal recombination. While laboratory-scale devices might work, scaling up WS₂ deposition and perovskite film quality could pose challenges. The sensitivity to moisture and potential thermal degradation limit long-term performance of (NH₄)₃Sb₂I₉ PSC. It is challenging to produce high-quality, uniform films and to scale them up for large-area devices. (NH₄)₃Sb₂I₉ materials dissolve well in ethanol, which is low-cost, low-toxicity, and eco-friendly solvent. [1]. Two-step method can be employed for the preparation of lead-free (NH₄)₃Sb₂I₉ PSC exhibits an enhanced PCE with high V_{oc} [2]. The structure presents a promising concept with the potential for innovative and high-performance solar cells. To experimentally improve the performance of PSCs, several key strategies are being explored. One major approach is material engineering, where the perovskite composition is carefully tuned such as incorporating mixed cations or halides to enhance light absorption, thermal stability, and reduce degradation. Additionally, the introduction of defect passivation agents helps to minimize non-radiative recombination by reducing trap states in the material. Interface optimization is another critical area; improving the quality and alignment of the ETLs and HTLs ensures efficient charge extraction and reduces energy losses. The use of interfacial layers can further enhance device stability and reduce performance hysteresis.

Chapter 5

Learning Through the Process of Research Paper Writing

Writing a research paper was not just a part of my academic requirement—it turned out to be a complete learning journey. From rejections to major revisions and finally getting accepted, every step taught me something important about doing and presenting scientific research.

6.1 Facing Initial Rejections

My first manuscript was rejected by two journals. It was disheartening, but it gave me perspective.

What I learned:

- Rejection is a normal part of research publishing.
- It's important to analyse reviewer feedback rather than take it personally.
- Good science also needs good presentation—clarity, structure, and relevance matter.

6.2 Submitting to *Physica Scripta*

Later, I submitted my manuscript to *Physica Scripta*, where the reviewers appreciated the novelty of the work—especially since it dealt with lead-free perovskite materials and had no prior simulation-based studies on it.

What I learned:

- Selecting the right journal for your topic is crucial.
- A strong introduction and justification of novelty can make your work stand out.
- Reviewers do value originality and research gaps.

6.3 Handling Major Revisions

The first round of review came with 32 detailed comments, mostly about material properties and result analysis. I addressed each of them carefully and revised both the manuscript and my understanding.

What I learned:

- Always read reviewer comments with a calm and open mindset.
- Each reviewer comment is an opportunity to strengthen the paper.
- Responding clearly, point-by-point, builds credibility.
- Good research also means being able to explain and defend your choices.

6.4 Final Round of Minor Revision

After my major revision, the referees accepted the paper with just **one minor correction**. I submitted a final update and a concise response.

What I learned:

- Attention to detail can be the difference between rejection and acceptance.
- Never rush responses; even minor comments need proper handling.
- Persistence pays off.

6.5 Final Acceptance and Key Takeaways

After multiple iterations, my paper was finally **accepted**. The process took time, but the journey was worth it.

What I learned from the entire experience:

- How to structure a research paper professionally.
- The importance of solid literature review and citing the right sources.
- How to communicate results clearly and meaningfully.
- How to write an effective “Response to Reviewer” document.
- That research writing is not just about results, but about how you present and support them.

Chapter 6

Conclusions

We studied performance of solar cell by evaluating combinations of different HTLs and ETLs. Our findings reveal that the PCE decreases as N_t increases, with an optimal efficiency of 19.51 % observed at a value of $N_t = 10^{13} \text{ cm}^{-3}$. Additionally, the PCE improved with increasing thickness, achieving optimal value of 20.08 % at thickness of 700 nm. Temperature also played a critical role, with the PCE steadily declining as temperature rose. The highest efficiency of 20.08 % was recorded at 300 K ($N_t = 10^{13} \text{ cm}^{-3}$). The influence of back contact materials was also examined. Pt, show top performance in both PCE and FF, but due to its high cost, Pt was deemed less commercially viable. Therefore, gold (Au) is chosen as the back electrode. Finally, the optimized device architecture is FTO/WS₂/(NH₄)₃Sb₂I₉/MASnBr₃/Au to achieve the maximum performance of device. This research highlights the promising potential of (NH₄)₃Sb₂I₉-based PSCs and underscores the importance of continued experimental studies to validate and expand upon these simulation-based findings. Future research can build upon the optimal parameters identified in this study to further enhance development of efficient and stable PSC.

References

- [1] A. Verma, N. Shrivastav, and J. Madan, "Enhancing Sustainability in Photovoltaic Technology: Optimization of $\text{NH}_2(\text{CH}_2)_2\text{NH}_3\text{MnCl}_4$ Perovskite Solar Cells," *2024 IEEE International Conference on Information Technology, Electronics and Intelligent Communication Systems, ICITEICS 2024*, p. 1, 2024, doi: 10.1109/ICITEICS61368.2024.10625166.
- [2] NRE Laboratory, "Best Research-Cell Efficiencies." Accessed: Dec. 30, 2024. [Online]. Available: <https://www.nrel.gov/pv/assets/images/efficiency-chart.png>
- [3] N. K. Noel *et al.*, "Lead-free organic-inorganic tin halide perovskites for photovoltaic applications," *Energy Environ Sci*, vol. 7, no. 9, pp. 3061–3068, 2014, doi: 10.1039/c4ee01076k.
- [4] L.-J. Chen, "Synthesis and optical properties of lead-free cesium germanium halide perovskite quantum rods†," *RSC Adv*, vol. 8, pp. 18396–18396, 2018, doi: 10.1039/c8ra01150h.
- [5] A. Singh *et al.*, "Panchromatic heterojunction solar cells for Pb-free all-inorganic antimony based perovskite," *Chemical Engineering Journal*, vol. 419, Sep. 2021, doi: 10.1016/j.cej.2021.129424.
- [5a] S. Yun, Y. Qin, A. R. Uhl, N. Vlachopoulos, M. Yin, D. Li, X. Han, and A. Hagfeldt, "New-generation integrated devices based on dye-sensitized and perovskite solar cells," *Energy & Environmental Science*, vol. 11, pp. 476–512, 2018.
- [6] M. Ikram *et al.*, "Recent advancements and future insight of lead-free non-toxic perovskite solar cells for sustainable and clean energy production: A review," Oct. 01, 2022, *Elsevier Ltd.* doi: 10.1016/j.seta.2022.102433.
- [7] X. Zhang *et al.*, "Germanium–lead double absorber layer perovskite solar cells: Further performance enhancement from the perspective of device simulation," *Opt Commun*, vol. 530, Mar. 2023, doi: 10.1016/j.optcom.2022.129188.
- [8] T. Krishnamoorthy *et al.*, "Lead-free germanium iodide perovskite materials for photovoltaic applications," *J Mater Chem A Mater*, vol. 3, no. 47, pp. 23829–23832, 2015, Accessed: Jan. 25, 2025. [Online]. Available: <https://doi.org/10.1039/C5TA05741H>
- [9] J.-P. Correa-Baena *et al.*, "A-Site Cation in Inorganic $\text{A}_3\text{Sb}_2\text{I}_9$ Perovskite Influences Structural Dimensionality, Exciton Binding Energy, and Solar Cell Performance," *Chemistry of Material*, vol. 30, pp. 3734–3742, 2018, Accessed: Dec. 30, 2024. [Online]. Available: <https://doi.org/10.1021/acs.chemmater.8b00676>
- [10] P. Kumar, K. Ahmad, J. Dagar, E. Unger, and S. M. Mobin, "Two-Step Deposition Approach for Lead Free $(\text{NH}_4)_3\text{Sb}_2\text{I}_9$ Perovskite Solar Cells with Enhanced Open Circuit Voltage and Performance," *ChemElectroChem*, vol. 8, no. 16, pp. 3150–3154, Aug. 2021, doi: 10.1002/celec.202100957.
- [11] D. Valli *et al.*, "Temperature-Dependent Evolution of the Structural and Optoelectronic Properties of $(\text{NH}_4)_3\text{Sb}_2\text{I}_9$ Single Crystals," *Journal of Physical Chemistry C*, vol. 127, no. 41, pp. 20419–20425, Oct. 2023, doi: 10.1021/acs.jpcc.3c05132.

- [12] L. Lin, L. Jiang, P. Li, B. Fan, and Y. Qiu, "A modeled perovskite solar cell structure with a Cu₂O hole-transporting layer enabling over 20% efficiency by low-cost low-temperature processing," *Journal of Physics and Chemistry of Solids*, vol. 124, pp. 205–211, Jan. 2019, doi: 10.1016/j.jpcs.2018.09.024.
- [13] P. C. Harikesh *et al.*, "Doping and Switchable Photovoltaic Effect in Lead-Free Perovskites Enabled by Metal Cation Transmutation," *Advanced Materials*, vol. 30, no. 34, p. 1802080, Aug. 2018, doi: 10.1002/ADMA.201802080.
- [14] C. Zuo and L. Ding, "Lead-free Perovskite Materials (NH₄)₃Sb₂I_xBr_{9-x}," *Angewandte Chemie*, vol. 129, no. 23, pp. 6628–6632, Jun. 2017, doi: 10.1002/ange.201702265.
- [15] A. A. Kanoun, M. B. Kanoun, A. E. Merad, and S. Goumri-Said, "Toward development of high-performance perovskite solar cells based on CH₃NH₃GeI₃ using computational approach," *Solar Energy*, vol. 182, pp. 237–244, Apr. 2019, doi: 10.1016/J.SOLENER.2019.02.041.
- [16] K. Deepthi Jayan and V. Sebastian, "Comprehensive device modelling and performance analysis of MASnI₃ based perovskite solar cells with diverse ETM, HTM and back metal contacts," *Solar Energy*, vol. 217, pp. 40–48, Mar. 2021, doi: 10.1016/J.SOLENER.2021.01.058.
- [17] X. Xu, J. Wang, D. Cao, Y. Zhou, and Z. Jiao, "Design of all-inorganic hole-transport-material-free CsPbI₃/CsSnI₃ heterojunction solar cells by device simulation," *Mater Res Express*, vol. 9, no. 2, 2022, doi: 10.1088/2053-1591/ac5778.
- [18] I. Montoya De Los Santos *et al.*, "Optimization of CH₃NH₃PbI₃ perovskite solar cells: A theoretical and experimental study," *Solar Energy*, vol. 199, pp. 198–205, Mar. 2020, doi: 10.1016/J.SOLENER.2020.02.026.
- [19] N. Lakhdar and A. Hima, "Electron transport material effect on performance of perovskite solar cells based on CH₃NH₃GeI₃," *Opt Mater (Amst)*, vol. 99, p. 109517, Jan. 2020, doi: 10.1016/J.OPTMAT.2019.109517.
- [20] S. Bhattacharai and T. D. Das, "Optimization of carrier transport materials for the performance enhancement of the MAGeI₃ based perovskite solar cell," *Solar Energy*, vol. 217, pp. 200–207, Mar. 2021, doi: 10.1016/J.SOLENER.2021.02.002.
- [21] A. A. Kanoun, M. B. Kanoun, A. E. Merad, and S. Goumri-Said, "Toward development of high-performance perovskite solar cells based on CH₃NH₃GeI₃ using computational approach," *Solar Energy*, vol. 182, pp. 237–244, Apr. 2019, doi: 10.1016/J.SOLENER.2019.02.041.
- [22] Himanshu, Kamlesh, D. Suthar, and M. S. Dhaka, "Numerical simulation of CdSe/ZnTe thin film solar cells by SCAPS-1D: Optimization of absorber layer thickness," *Solid State Commun*, vol. 371, Oct. 2023, doi: 10.1016/j.ssc.2023.115264.
- [23] O. Skhouni, A. El Manouni, M. Mollar, R. Schrebler, and B. Marí, "ZnTe thin films grown by electrodeposition technique on Fluorine Tin Oxide substrates," *Thin Solid Films*, vol. 564, pp. 195–200, Aug. 2014, doi: 10.1016/j.tsf.2014.06.002.

- [24] F. Azri, A. Meftah, N. Sengouga, and A. Meftah, "Electron and hole transport layers optimization by numerical simulation of a perovskite solar cell," *Solar Energy*, vol. 181, pp. 372–378, Mar. 2019, doi: 10.1016/j.solener.2019.02.017.
- [25] Y. Gan *et al.*, "Numerical investigation energy conversion performance of tin-based perovskite solar cells using cell capacitance simulator," *Energies (Basel)*, vol. 13, no. 22, Nov. 2020, doi: 10.3390/en13225907.
- [26] X. Meng *et al.*, "Optimization of germanium-based perovskite solar cells by SCAPS simulation," *Opt Mater (Amst)*, vol. 128, Jun. 2022, doi: 10.1016/j.optmat.2022.112427.
- [27] Naureen, Sadanand, P. Lohia, D. Dwivedi, and S. Ameen, "A Comparative Study of Quantum Dot Solar Cell with Two Different ETLs of WS₂ and IGZO Using SCAPS-1D Simulator," *Solar*, vol. 2, no. 3, pp. 341–353, Aug. 2022, doi: 10.3390/solar2030020.
- [28] M. K. Hossain *et al.*, "An extensive study on multiple ETL and HTL layers to design and simulation of high-performance lead-free CsSnCl₃-based perovskite solar cells," *Sci Rep*, vol. 13, no. 1, Dec. 2023, doi: 10.1038/s41598-023-28506-2.
- [29] U. Mandadapu, S. V. Vedanayakam, and K. Thyagarajan, "Simulation and Analysis of Lead based Perovskite Solar Cell using SCAPS-1D," *Indian J Sci Technol*, vol. 10, no. 1, pp. 1–8, Jan. 2017, doi: 10.17485/ijst/2017/v11i10/110721.
- [30] P. K. Bhujbal *et al.*, "Unlocking the Potential of WS₂ as an Electron Transport Layer in Flexible and Lead-Free Methylammonium Tin Iodide -Based Perovskite Solar Cells: A Comprehensive Defect Study Using the SCAPS-1D Framework," *ES Energy & Environment*, vol. 26, 2024, doi: 10.30919/ese1225.
- [31] W. Ke and M. G. Kanatzidis, "Prospects for low-toxicity lead-free perovskite solar cells," Dec. 01, 2019, *Nature Publishing Group*. doi: 10.1038/s41467-019-08918-3.
- [32] A. Abate, "Perovskite Solar Cells Go Lead Free," Dec. 20, 2017, *Cell Press*. doi: 10.1016/j.joule.2017.09.007.
- [33] H. Yao, F. Zhou, Z. Li, Z. Ci, L. Ding, and Z. Jin, "Strategies for Improving the Stability of Tin-Based Perovskite (ASnX₃) Solar Cells," May 01, 2020, *John Wiley and Sons Inc*. doi: 10.1002/advs.201903540.
- [34] Y. M. Lee *et al.*, "Comprehensive Understanding and Controlling the Defect Structures: An Effective Approach for Organic-Inorganic Hybrid Perovskite-Based Solar-Cell Application," Nov. 29, 2018, *Frontiers Media S.A.* doi: 10.3389/fenrg.2018.00128.
- [35] M. Lazemi, S. Asgharizadeh, and S. Bellucci, "A computational approach to interface engineering of lead-free CH₃NH₃SnI₃ highly-efficient perovskite solar cells," *Physical Chemistry Chemical Physics*, vol. 20, no. 40, pp. 25683–25692, Oct. 2018, doi: 10.1039/C8CP03660H.
- [36] R. Kundara and S. Baghel, "Performance analysis of LaFeO₃ perovskite solar cells: A theoretical and experimental study," *Solid State Commun*, vol. 389, Oct. 2024, doi: 10.1016/j.ssc.2024.115590.
- [37] M. S. Jamal *et al.*, "Effect of defect density and energy level mismatch on the performance of perovskite solar cells by numerical simulation," *Optik (Stuttg)*, vol. 182, pp. 1204–1210, Apr. 2019, doi: 10.1016/j.ijleo.2018.12.163.

- [38] M. Lazemi, S. Asgharizadeh, and S. Bellucci, "A computational approach to interface engineering of lead-free $\text{CH}_3\text{NH}_3\text{SnI}_3$ highly-efficient perovskite solar cells," *Physical Chemistry Chemical Physics*, vol. 20, no. 40, pp. 25683–25692, Oct. 2018, doi: 10.1039/C8CP03660H.
- [39] D. Y. Son, J. H. Im, H. S. Kim, and N. G. Park, "11% efficient perovskite solar cell based on ZnO nanorods: An effective charge collection system," *Journal of Physical Chemistry C*, vol. 118, no. 30, pp. 16567–16573, Jul. 2014, doi: 10.1021/JP412407J/ASSET/IMAGES/MEDIUM/JP-2013-12407J_0013.GIF.
- [40] R. Kundara and S. Baghel, "Device modelling of lead free $(\text{CH}_3\text{NH}_3)_2\text{CuX}_4$ based perovskite solar cells using SCAPS simulation," *Opt Quantum Electron*, vol. 55, no. 11, Nov. 2023, doi: 10.1007/s11082-023-05244-3.
- [41] Md. S. Uddin, R. Hosen, S. Sikder, H. Mamur, and M. R. A. Bhuiyan, "Photovoltaic performance enhancement of $\text{Al}/\text{ZnO}:\text{Al}/\text{i-ZnO}/\text{CdS}/\text{CIGS}/\text{Pt}$ solar cell using SCAPS-1D software," *Next Energy*, vol. 2, p. 100080, Jan. 2024, doi: 10.1016/j.nxener.2023.100080.
- [42] E. L. Meyer, S. Jakalase, A. Nqombolo, N. Rono, and M. A. Agoro, "The Numerical Simulation of a Non-Fullerene Thin-Film Organic Solar Cell with $\text{Cu}_2\text{FeSnS}_4$ (CFTS) Kesterite as a Hole Transport Layer Using SCAPS-1D," *Coatings*, vol. 15, no. 3, p. 266, Feb. 2025, doi: 10.3390/coatings15030266.
- [43] M. Kevin, W. L. Ong, G. H. Lee, and G. W. Ho, "Formation of hybrid structures: Copper oxide nanocrystals templated on ultralong copper nanowires for open network sensing at room temperature," *Nanotechnology*, vol. 22, no. 23, Jun. 2011, doi: 10.1088/0957-4484/22/23/235701.
- [44] T. Ghrib *et al.*, "Annealing effect on the microstructural, optical, electrical, and thermal properties of $\text{Cu}_2\text{O}/\text{TiO}_2/\text{Cu}_2\text{O}/\text{TiO}_2/\text{Si}$ heterojunction prepared by sol-gel technique," *Micro and Nanostructures*, vol. 164, p. 107119, Apr. 2022, doi: 10.1016/J.SPMI.2021.107119.
- [45] K. Ahmad, M. Q. Khan, and H. Kim, "Simulation and fabrication of all-inorganic antimony halide perovskite-like material based Pb-free perovskite solar cells," *Opt Mater (Amst)*, vol. 128, p. 112374, Jun. 2022, doi: 10.1016/J.OPTMAT.2022.112374.
- [46] M. T. Islam *et al.*, "Numerical simulation studies of $\text{Cs}_3\text{Bi}_2\text{I}_9$ perovskite solar device with optimal selection of electron and hole transport layers," *Optik (Stuttg)*, vol. 231, p. 166417, Apr. 2021, doi: 10.1016/J.IJLEO.2021.166417.
- [47] H. Zhang *et al.*, "Improving the stability and performance of perovskite solar cells via off-the-shelf post-device ligand treatment," *Energy Environ Sci*, vol. 11, no. 8, pp. 2253–2262, Aug. 2018, doi: 10.1039/C8EE00580J.
- [48] International Energy Agency, *Share of renewable electricity generation by technology, 2000–2030*, IEA, Paris, 2024. [Online]. Available: <https://www.iea.org/data-and-statistics/charts/share-of-renewable-electricity-generation-by-technology-2000-2030>
- [49] P. G. V. Sampaio and M. O. A. González, "Photovoltaic solar energy: Conceptual framework," *Renewable and Sustainable Energy Reviews*, vol. 74, pp. 590–601, 2017.

APPENDICES

A.1 PROOF OF SUBMISSION AND STATUS OF PAPER

ScholarOne Manuscripts™ Sumit Singh Instructions, Forms & Policies Help Log Out

IOP Physica Scripta now required for submission

[Home](#) [Author](#) [Review](#)

Author Dashboard

Author Dashboard

- 3 Manuscripts I Have Co-Authored
- [Start New Submission](#)
- [5 Most Recent E-mails](#)

Manuscripts I Have Co-Authored

To contact the journal team about a specific article please email physscr@iopublishing.org, quoting the Manuscript ID.

An ORCID ID is now required for all submitting authors on this journal. For more information on ORCID and why an ORCID ID is important, visit <https://orcid.org/>

STATUS	ID	TITLE	CREATED	SUBMITTED
<ul style="list-style-type: none"> Formal Accept (02-Jun-2025) Accepted - Preparing for Production 	PHYSSCR-140802.R2	Device modelling and optimization of new lead-free (NH ₄) ₃ Sb ₂ I ₉ perovskite solar cells by using SCAPS-1D software View Submission Submitting Author: Kundara, Rahul	22-May-2025	22-May-2025
<ul style="list-style-type: none"> Minor Revision (21-May-2025) a revision has been submitted 	PHYSSCR-140802.R1	Device modelling and optimization of new lead-free (NH ₄) ₃ Sb ₂ I ₉ perovskite solar cells by using SCAPS-1D software View Submission Submitting Author: Kundara, Rahul	25-Apr-2025	25-Apr-2025
<ul style="list-style-type: none"> Major Revision (03-Apr-2025) a revision has been submitted 	PHYSSCR-140802	Device modelling and optimization of new lead-free (NH ₄) ₃ Sb ₂ I ₉ perovskite solar cells by using SCAPS-1D software View Submission Submitting Author: Kundara, Rahul	15-Mar-2025	15-Mar-2025

Status: Accepted



Sumit Singh <singhmit0912@gmail.com>

Your manuscript PHYSSCR-140802.R2 has been accepted for publication

1 message

Physica Scripta <onbehalf@manuscriptcentral.com>

2 June 2025 at 18:23

Reply-To: physscr@iopublishing.org

To: singhmit0912@gmail.com, rahul_2k20phdap10@dtu.ac.in, saritabaghel@dtu.ac.in

Dear Mr Kundara,

Re: "Device modelling and optimization of new lead-free (NH₄)₃Sb₂I₉ perovskite solar cells by using SCAPS-1D software"

Manuscript reference: PHYSSCR-140802.R2

We are pleased to tell you that we are accepting your Paper. We now have everything we need to publish it in Physica Scripta.

You can find more information about your accepted manuscript on our [Publishing Support](#) website.

You will receive a confirmation email which will include the [Digital Object Identifier](#). This should be used for citing your work.

DATA AVAILABILITY

The proof of your article will contain an automatically-generated data availability statement based on your answer to the data availability question on the submission form. Please ensure you check the proof for the correct data citation and consistency with any other mention(s) of data availability within the manuscript itself to avoid contradiction.

If you have opted to use IOP Publishing's Figshare repository to make your data openly available this has now been verified and the DOI will be automatically inserted into the proof of your article.

Next steps

We will email again when article proofs are ready for your final approval. Please return them by the date given in that email so that we can produce the final published version without delay.

ACCEPTED MANUSCRIPT

Device modelling and optimization of new lead-free $(\text{NH}_4)_3\text{Sb}_2\text{I}_9$ perovskite solar cells by using SCAPS-1D software

Sumit Singh, Rahul Kundara and Sarita Baghel

Accepted Manuscript online 2 June 2025 • © 2025 IOP Publishing Ltd. All rights, including for text and data mining, AI training, and similar technologies, are reserved.

[What is an Accepted Manuscript?](#)

DOI 10.1088/1402-4896/addfba


[Authors](#) ▼

[Article information](#) ▼

Article metrics

1 Total downloads

Submit

[Submit to this Journal](#)

Permissions

[Get permission to re-use this article](#)

Share this article






Abstract

Advancing lead-free perovskite solar cells (PSCs) is essential for developing sustainable and eco-friendly solar technologies. These alternatives to lead-based PSCs offer notable benefits, including low-cost, excellent stability, and promising efficiency, positioning them as attractive candidates for next-generation photovoltaic applications. Among the emerging materials, $(\text{NH}_4)_3\text{Sb}_2\text{I}_9$ stands out due to its favourable optoelectronic properties and environmental safety. This study investigates the impact of different HTLs and ETLs on the performance of $(\text{NH}_4)_3\text{Sb}_2\text{I}_9$ -based devices using SCAPS-1D software. Several parameters influencing device efficiency were optimized, including thickness of absorber layer, operating temperature, work function of back contact, donor density, defect density (Nt), series and shunt resistance. The optimized device structure, FTO/WS₂/(NH_4)₃Sb₂I₉/MASnBr₃/Au achieved a PCE of 20.08 % with a VOC of 1.65 V, JSC of 13.83 mA/cm² and FF of 87.93 % at 300 K and Nt of 1013 cm⁻³. These results demonstrate the strong potential of antimony-based perovskites in the development of high-performance, lead-free solar cells.

Abstract

[↑ Back to top](#)

A.2 PROOF OF SCI/SCOPUS/SCIE INDEXING

PHYSICA SCRIPTA

Publisher: IOP PUBLISHING LTD, TEMPLE CIRCUS, TEMPLE WAY, BRISTOL, ENGLAND, BS1 6BE

ISSN / eISSN: 0031-8949 / 1402-4896

Web of Science Core Collection: Science Citation Index Expanded

Additional Web of Science Indexes: Current Contents Physical, Chemical & Earth Sciences | Essential Science Indicators

[Share This Journal](#)

[View profile page](#)

A.3 PLAGIARISM REPORT

Sumit

24-25 Thesis_Report_sumit.pdf

 Delhi Technological University

Document Details

Submission ID

trn:oid::27535:99807461

Submission Date

Jun 8, 2025, 7:11 AM GMT+5:30

Download Date

Jun 8, 2025, 7:17 AM GMT+5:30

File Name

24-25 Thesis_Report_sumit.pdf

File Size

4.9 MB

54 Pages

11,497 Words

59,752 Characters



Page 2 of 59 - Integrity Overview

Submission ID trn:oid::27535:99807461

9% Overall Similarity

The combined total of all matches, including overlapping sources, for each database.





Filtered from the Report

- Bibliography
- Quoted Text
- Cited Text
- Small Matches (less than 10 words)

Exclusions

- 1 Excluded Source

Match Groups

-  **54 Not Cited or Quoted 9%**
Matches with neither in-text citation nor quotation marks
-  **0 Missing Quotations 0%**
Matches that are still very similar to source material
-  **0 Missing Citation 0%**
Matches that have quotation marks, but no in-text citation
-  **0 Cited and Quoted 0%**
Matches with in-text citation present, but no quotation marks

Top Sources

- 6%  Internet sources
- 4%  Publications
- 7%  Submitted works (Student Papers)

Integrity Flags

0 Integrity Flags for Review

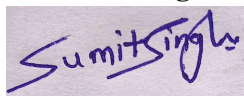
No suspicious text manipulations found.

Our system's algorithms look deeply at a document for any inconsistencies that would set it apart from a normal submission. If we notice something strange, we flag it for you to review.

A Flag is not necessarily an indicator of a problem. However, we'd recommend you focus your attention there for further review.

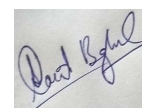
Sumit Singh (23/MSCPHY/47)

Candidate's Signature



Dr. Sarita Baghel

(Signature of Supervisor)





Match Groups

- **54 Not Cited or Quoted 9%**
Matches with neither in-text citation nor quotation marks
- **0 Missing Quotations 0%**
Matches that are still very similar to source material
- **0 Missing Citation 0%**
Matches that have quotation marks, but no in-text citation
- **0 Cited and Quoted 0%**
Matches with in-text citation present, but no quotation marks

Top Sources

- 6% ■ Internet sources
- 4% ■ Publications
- 7% ■ Submitted works (Student Papers)

Top Sources

The sources with the highest number of matches within the submission. Overlapping sources will not be displayed.

1	Internet	
dspace.dtu.ac.in:8080		3%
2	Internet	
dtu.ac.in		<1%
3	Publication	
Revathy Raghunathan Lekshmy, Ehsan Raza, Zubair Ahmad, Jolly Bhadra. "Simula...		<1%
4	Submitted works	
Indian School of Mines on 2025-05-01		<1%
5	Publication	
Rahul Kundara, Sarita Baghel. "Performance optimization of lead-free KGeCl3 bas...		<1%
6	Internet	
www.mdpi.com		<1%
7	Internet	
www.dspace.dtu.ac.in:8080		<1%
8	Submitted works	
University of Northumbria at Newcastle on 2025-05-08		<1%